Late Cenozoic exhumation of the Cascadia accretionary wedge in the Olympic Mountains, northwest Washington State

Mark T. Brandon* *Department of Geology and Geophysics, Yale University, P.O. Box 208109, New Haven, Connecticut 06520-8109*

Mary K. Roden-Tice† *Department of Earth and Environmental Science, Rensselaer Polytechnic Institute, Troy, New York 12180-3590*

John I. Garver§ *Geology Department, Union College, Schenectady, New York 12308-2311*

ABSTRACT

The apatite fission-track method is used to determine the exhumation history of the Olympic subduction complex, an uplifted part of the modern Cascadia accretionary wedge. Fission-track ages are reported for 35 sandstones from the Olympic subduction complex, and 7 sandstones and 1 diabase from the Coast Range terrane, which structurally overlies the Olympic subduction complex. Most sandstone samples give discordant results, which means that the variance in grains ages is much greater than would be expected for radioactive decay alone. Discordance in an unreset sample is caused by a mix of detrital ages, and in a reset sample is caused by a mix of annealing properties among the detrital apatites and perhaps by U loss from some apatites. Discordant grain-age distributions can be successfully interpreted by using the minimum age, which is the pooled age of the youngest group of concordant fission-track grain ages in a dated sample. The inference is that this fraction of apatites has the lowest thermal stability, and will be the first to reset on heating and the last to close on cooling. Comparison of the minimum age with depositional age provides a simple distinction between reset samples (minimum age younger than deposition) and unreset samples (minimum age older than deposition). The success of the minimum-age approach is demonstrated by its ability to resolve a well-defined age-elevation trend for reset samples from the Olympic subduction complex. Microprobe data suggest that the apatites that make up the minimum-age fraction are mostly fluorapatite, which has the lowest thermal stability for fission tracks among the common apatites.

Reset minimum ages are all younger than 15 Ma, and show a concentric age pattern; the youngest ages are centered on the central massif of the Olympic Mountains and progressively older ages in the surrounding lowlands. Unreset localities are generally found in coastal areas, indicating relatively little exhumation there. Using a stratigraphically coordinated suite of apatite fission-track ages, we estimate that prior to the start of exhumation, the base of the fluorapatite partial annealing zone was located at ~100 °C and ~4.7 km depth. The temperature gradient at that time was 19.6 ± 4.4 °C/km, similar to the modern gradient in adjacent parts of the Cascadia forearc high.

Apatite and previously published zircon fission-track data are used to determine the exhumation history of the central massif. Sedimentary rocks exposed there were initially accreted during late Oligocene and early Miocene time at depths of 12.1–14.5 km and temperatures of ~242–289 °C. Exhumation began at ca. 18 Ma. A rock currently at the local mean elevation of the central massif (1204 m) would have moved through the α-damaged zircon closure temperature at about 13.7 Ma and ~10.0 km depth, and through the fluorapatite closure temperature at about 6.7 Ma and ~4.4 km depth. On the basis of age-elevation trends and paired cooling ages, we find that the exhumation rate in the central massif has remained fairly constant, ~0.75 km/m.y., since at least 14 Ma. Apatite fission-track data are used to construct a contour map of long-term exhumation rates for the Olympic Peninsula. The average rate for the entire peninsula is ~0.28 km/m.y., which is comparable with modern erosion rates (0.18 to 0.32 km/m.y.) estimated from sediment yield data for two major rivers of the Olympic Mountains.

We show that exhumation of this part of the Cascadia forearc high has been dominated by erosion and not by extensional faulting. Topography and erosion appear to have been sustained by continued accretion and thickening within the underlying Cascadia accretionary wedge. The rivers that drain the modern Olympic Mountains indicate that most of the eroded sediment is transported into the Pacific Ocean, where it is recycled back into the accretionary wedge, either by tectonic accretion or by sedimentary accumulation in shelf and slope basins. The influx of accreted sediments is shown to be similar to the outflux of eroded sediment, indicating that the Olympic segment of the Cascadia margin is currently close to a topographic steady state. The record provided by our fission-track data, of a steady exhumation rate for the central massif area since 14 Ma, suggests that this topographic steady state developed within several million years after initial emergence of the forearc high.

INTRODUCTION

Much of the forearc region of the Cascadia margin is subaerially exposed; the highest topography coincides with a coastal mountain range (Fig. 1A) extending from the Klamath Mountains of northern California and southwestern Oregon, the Coast Range of western Oregon and Wash-

*E-mail: mark.brandon@yale.edu.

†Present address: Center for Earth and Environmental Sciences, State University of New York at Plattsburgh, Plattsburgh, New York 12901; e-mail: rodentmk@splava.cc.plattsburgh.edu.

§E-mail: garverj@idol.union.edu.

Data Repository item 9865 contains additional material related to this article.

GSA Bulletin; August 1998; v. 110; no. 8; p. 985–1009; 18 figures; 3 tables.

ington, and the Insular Range of Vancouver Island. This high separates a relatively continuous forearc depression to the east (Willamette, Puget and Georgia lowlands in Fig. 1A) from the accretionary wedge offshore to the west. The Cascadia forearc high is similar to uplifted forearc highs found at other mature continental convergent margins, such as Kodiak Island of the east Aleutian margin, Shikoku of the southeast Japan margin, the Island of Crete of the Hellenic margin, southern Iraq and western Pakistan of the Makran margin, and northeast New Zealand of the Hikurangi margin. Dickinson and Seely (1979) referred to these as ridged forearcs. Ancient subduction complexes also show evidence of ridged forearc highs, such as the Franciscan Complex of California, which became emergent during Late Cretaceous and Paleogene time (Dickinson and Seely, 1979).

A much debated issue these days is the formation and exhumation of high-pressure metamorphic rocks, the forearc high being a common site where these rocks are unroofed. The margin beneath most ridged forearc highs is commonly thick enough to produce high-pressure metamorphic rocks. For example, the Olympic Mountains are underlain by ~30 km of accreted sedimentary rocks (Brandon and Calderwood, 1990), which indicates metamorphic pressures of as much as 800 Mpa. A critical question is how these rocks are returned to the surface. One popular interpretation is that exhumation occurs primarily by tectonic processes, such as normal faulting and ductile thinning (e.g., Platt, 1986, 1987, 1993; Jayko et al., 1987; Cashman and Kelsey, 1990; Harms et al., 1992; Wallis et al., 1993). Erosion must also play a role, but its contribution has received less attention.

In this paper we use detailed fission-track data from the Olympic subduction complex to study exhumation processes operating in the Olympic Mountains. Uplift and erosion are active along the entire length of the Cascadia forearc high. The Olympic Mountains appear to have been the first area to have emerged above sea level, starting in Miocene time (Brandon and Calderwood, 1990); at present, this area shows the greatest exhumation. The inference is that with time, the rest of the Cascadia forearc will follow a similar history, assuming continued uplift beneath the forearc high. Thus, our local results provide important insights for how exhumation might occur at emergent forearc highs at other convergent margins.

In a previous study, Brandon and Vance (1992) identified a small area within the central and most elevated part of the Olympic Mountains where detrital zircons in sandstones of the Olympic subduction complex were reset to a fission-track age of about 14 Ma. They estimated a maximum depth of exhumation of ~12 km and an average exhumation rate of ~1 km/m.y. However, zircon fission-track ages provide only a restricted view of exhumation in the Olympic Mountains because the reset area for zircon is so small. We anticipated that apatite fission-track ages would give a broader picture of the pattern and rates of exhumation, given that apatite has a lower closure temperature, ~110 °C, relative to that for zircon, which is ~240 °C.

In this paper we report 43 new apatite fission-track ages for locations covering most of the Olympic Peninsula.[1] These data are used to (1) determine a detailed exhumation history for the central part of the Olympic Mountains uplift; (2) map out the regional pattern of exhumation in order to identify potential structural breaks produced by extensional faulting; and (3) compare average long-term exhumation rates with modern erosion rates.

REGIONAL SETTING

The Cascadia forearc is underlain by four tectonostratigraphic units (Fig. 2) (Brandon and Vance, 1992). The two inboard units, labeled pre-Tertiary continental framework and displaced Mesozoic terranes, were assembled along the North America margin during Late Cretaceous and Paleogene time. Subsequent accretion has added two outboard units: the Coast Range terrane and the Cascadia accretionary wedge.

The Coast Range terrane extends over a distance of 750 km, from southwest Oregon to the continental shelf west of central Vancouver Island (Wells et al., 1984; Clowes et al., 1987). It consists of a thick fault-bounded slab of lower Eocene oceanic crust and an overlying marine clastic sequence, informally known as the Peripheral sequence. The ophiolitic basement of the Coast Range terrane may have originated by collision of an intra-Pacific seamount province or by backarc or forearc rifting at the North American margin (Wells et al., 1984; Clowes et al., 1987; Babcock et al., 1992). The suture boundary along the inboard side of the Coast Range terrane is not exposed, except on southernmost Vancouver Island, where it corresponds to the Leech River fault. Crosscutting relations exposed there broadly delimit suturing to between 42 and 24 Ma (Brandon and Vance, 1992). The Leech River fault may have been active during late Eocene time, as indicated by conglomerates shed southwestward from uplifted pre-Tertiary rocks north of the Leech River fault on Vancouver Island. The conglomerates are found in the Lyre Formation, which is exposed in the Peripheral sequence on the north side of the Olympic Peninsula. The Lyre has a depositional age of about 38 Ma (unreset fission-track minimum age for detrital zircons, reported in Garver and Brandon, 1994).

The Cascadia accretionary wedge formed outboard of the Coast Range terrane and has grown by frontal accretion and underplating (Clowes et al., 1987; Brandon and Calderwood, 1990). It underlies most of the offshore continental margin and is locally uplifted and exposed in the Olympic Mountains (Stewart, 1970; Rau, 1973; Tabor and Cady, 1978a, 1978b), where it is known as the Olympic subduction complex (Brandon and Vance, 1992) (Fig. 2).

The modern configuration of the margin, including a subduction zone west of the Coast Range terrane, was considered by Brandon and Vance (1992) to have originated in latest Eocene time (ca. 35 Ma). This interpretation contrasts with earlier syntheses that infer initiation of Cascadia subduction at ca. 50 Ma (e.g., Wells et al., 1984; Heller et al., 1987; Snavely, 1987). A ca. 35 Ma initiation is indicated by: (1) the ca. 38 Ma suturing of the Coast Range terrane to the continental framework along the Leech River fault;

[1]GSA Data Repository item 9865, location, geographic setting, and fission-track data for apatite samples, is available on request from Documents Secretary, GSA, P.O. Box 9140, Boulder, CO 80301. E-mail: editing@geosociety.org.

Figure 1. Topography and tectonic features of (A) the Cascadia margin from northern Oregon to southern Vancouver Island, and (B) the Olympic Peninsula. Solid black lines mark major faults (see Fig. 2 for names). The solid red line marks the western limit of Cascade volcanism (35 Ma to present). Red triangles indicate the modern Cascade volcanoes. Blue lines show the major rivers of western Washington. For (B), the dashed red lines enclose young basins surrounding the Olympic Mountains uplift, and the black dotted line shows the shelf edge. Abbreviations: Lw.—lower; Up.—upper; CRT—Coast Range terrane; OSC—Olympic subduction complex; PL—Puget Lowland, SJF—Straits of Juan de Fuca; WL—Willamette lowland; GL—Georgia lowland; NF—Nitnat submarine fan; and AF—Astoria submarine fan. Modern relative convergence velocity is from Nishimura et al. (1984). Figures were prepared using the GMT programs (Wessel and Smith, 1991) and digital topography from the DNAG CD-ROM (National Geophysical Data Center, 1989; spatial resolution is 30 arc seconds onland and coarser offshore).

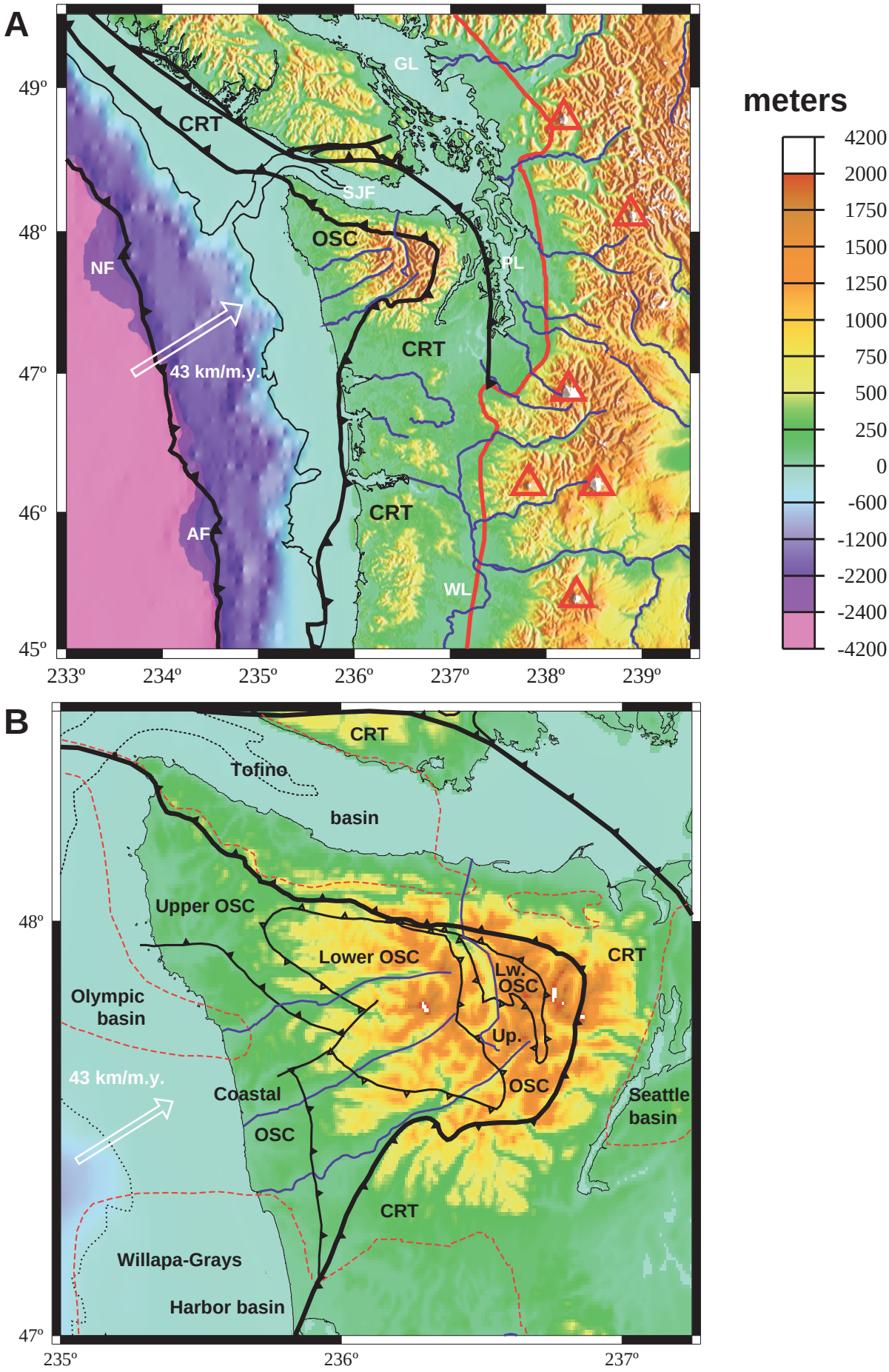
A
49º
48º
47º
46º
45º
233º
234º
235º
236º
237º
238º
239º
CRT
GL
SJF
OSC
NF
PL
CRT
43 km/m.y.
CRT
AF
WL
meters
4200
2000
1750
1500
1250
1000
750
500
250
0
-600
-1200
-2200
-2400
-4200
B
CRT
Tofino
basin
48º
Upper OSC
Lower OSC
Lw.
OSC
CRT
Olympic
basin
Up.
OSC
43 km/m.y.
Coastal
OSC
Seattle
basin
CRT
Willapa-Grays
Harbor basin
47º
235º
236º
237º

(2) the initiation of the Cascade volcanic arc at ca. 36 Ma (Armstrong and Ward, 1991; Brandon and Vance, 1992), and (3) the timing of slip on the Hurricane Ridge fault in the Olympic Mountains (Fig. 2). This fault marks the boundary between the Coast Range terrane and the outboard Olympic subduction complex. The age of the Hurricane Ridge fault is constrained by the age of the Needles–Gray Wolf assemblage, a unit in the Olympic subduction complex that directly underlies the fault. Brandon and Vance (1992) showed that clastic sediments of the Needles–Gray Wolf are ca. 33–39 Ma in age. From this we infer that some, if not all, of the slip on the Hurricane Ridge fault is latest Eocene or younger in age.

After initiation of the Cascadia subduction zone, plate convergence proceeded in a fairly steady and continuous fashion, as indicted by plate reconstructions (Engebretson et al., 1985; Lonsdale, 1988; Wilson, 1988) and the volcanic record of the Cascade arc (Smith, 1989; Sherrod and Smith, 1989). The subduction process has been dominated by the accretion of trench sediment; there is no evidence for collision of large seamounts or oceanic plateaus (Brandon and Calderwood, 1990; Brandon and Vance, 1992).

LOCAL GEOLOGY

Coast Range Terrane

In the Olympic Peninsula, the basal unit of the Coast Range terrane is the Crescent Formation (Fig. 3), which is made up of pillowed and massive basaltic flows, locally cut by diabase dikes and interbedded with rare pelagic limestone

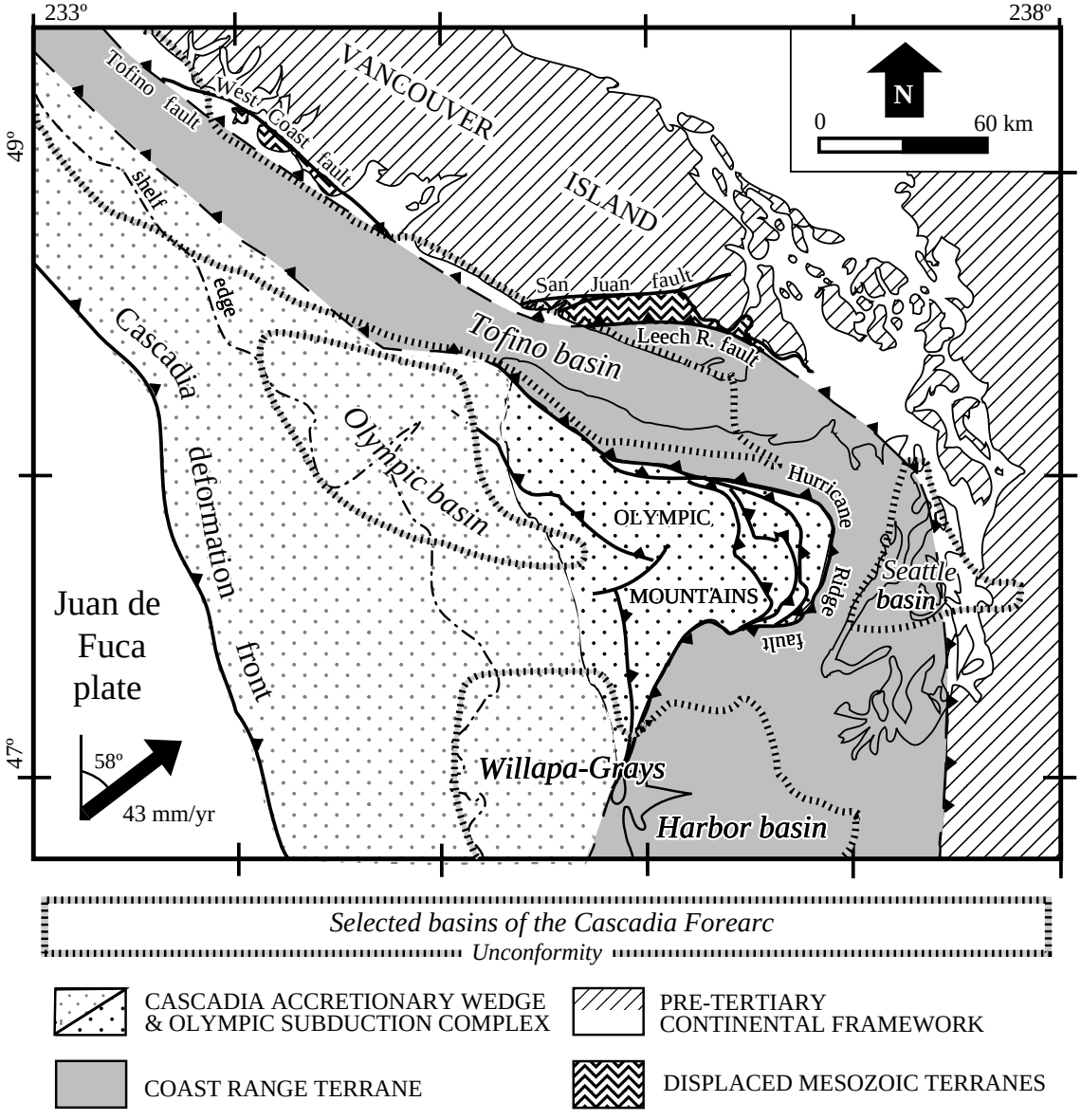

Figure 2. Generalized geologic map of the Cascadia margin in western Washington and southern Vancouver Island. The ruled lines enclose the modern basins (Miocene and younger) of the Cascadia forearc (after Shouldice, 1971; Muller, 1977; Tabor and Cady, 1978a; Snavely, 1987; Johnson et al., 1994).

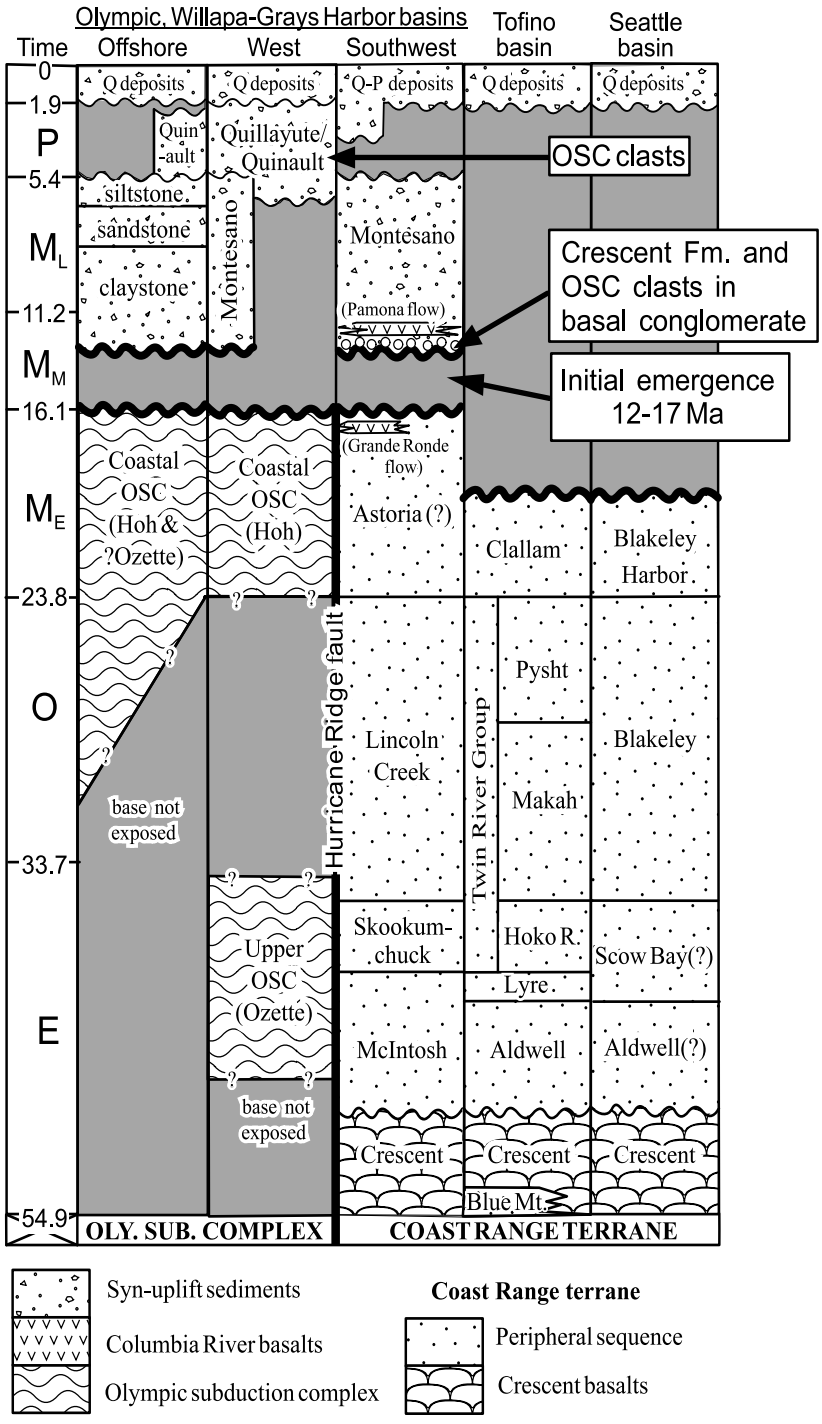

Figure 3. Summary of stratigraphic evidence for emergence and erosion of the Olympic Mountains starting in middle Miocene time. The locations of the cited basins are shown in Figure 2. Data sources: Offshore and West columns: Rau (1975, 1979), Snavely et al. (1986, 1993), Palmer and Lingley (1989); Southwest column: Armentrout et al. (1983, 1988), Walsh et al. (1987); Tofino column: Snavely et al. (1980), Garver and Brandon (1994); Seattle column: Armentrout et al. (1983, 1988), Squires et al. (1992), Johnson et al. (1994). OSC—Olympic subduction complex; E—Eocene; O—Oligocene; M—Miocene (E—early, M—middle, L—late); P—Paleocene; Fm.—formation; Q—Quaternary.

and reddish mudstone (Tabor and Cady, 1978a; Suczek et al., 1994). Its present thickness, ranging from 2 to 15 km, is largely a result of faulting that truncated the base of the unit and probably caused some internal imbrication as well.

Disconformably overlying the Crescent is the Peripheral sequence (Fig. 3), which is made up of Eocene through lower Miocene marine clastic strata, locally ~6 km thick (Tabor and Cady, 1978a; Snavely et al., 1980, 1993; Armentrout, 1987; Garver and Brandon, 1994). The Peripheral sequence is preserved in topographic and structural lows that surround the Olympic Mountains uplift, such as the Tofino and Seattle basins, and the eastern half of the Willapa–Grays Harbor basin (Figs. 1B and 2).

In most parts of the Oregon-Washington Coast Range, the Coast Range terrane typically has a gentle to horizontal attitude. However, adjacent to the Olympic Mountains, the terrane is steeply dipping and locally overturned (Tabor and Cady, 1978a, 1978b). The steep attitude of the Coast Range terrane outlines the modern topography of the Olympic Mountains (Fig. 1B) and reflects prolonged uplift and exhumation in that area. The Peripheral sequence is generally concordant with the underlying Crescent Formation, which indicates that the present steep attitude of the Coast Range terrane around the Olympic Mountains postdates deposition of the Peripheral sequence.

Olympic Subduction Complex

The Olympic subduction complex is exposed in the core of the Olympic uplift and is separated from the overlying Coast Range terrane by the Hurricane Ridge fault (Figs. 2 and 4). Tabor and Cady (1978a, 1978b) defined five major lithotectonic units within the Olympic subduction complex, based mainly on sandstone petrology, and to a lesser extent on age and deformational style. From east to west, their units are the Needles–Gray Wolf, Grand Valley, Elwha, Western Olympic, and Hoh lithic assemblages (Fig. 4).

Age-diagnostic fossils are very rare in most clastic units of the Olympic subduction complex, except for the Hoh unit. Brandon and Vance (1992) used fission-track grain ages from unreset detrital zircons to estimate the depositional ages of sandstones within the Olympic subduction complex. "Unreset" means that the zircons retain predepositional fission-track ages related to cooling events in their source region. Some simple criteria can be applied to identify samples having unreset zircon fission-track ages from those that were reset by high temperatures after deposition (see Brandon and Vance, 1992, for details). Samples with unreset zircons were shown to contain a significant fraction of young zircons, probably derived from a contemporaneous volcanic source

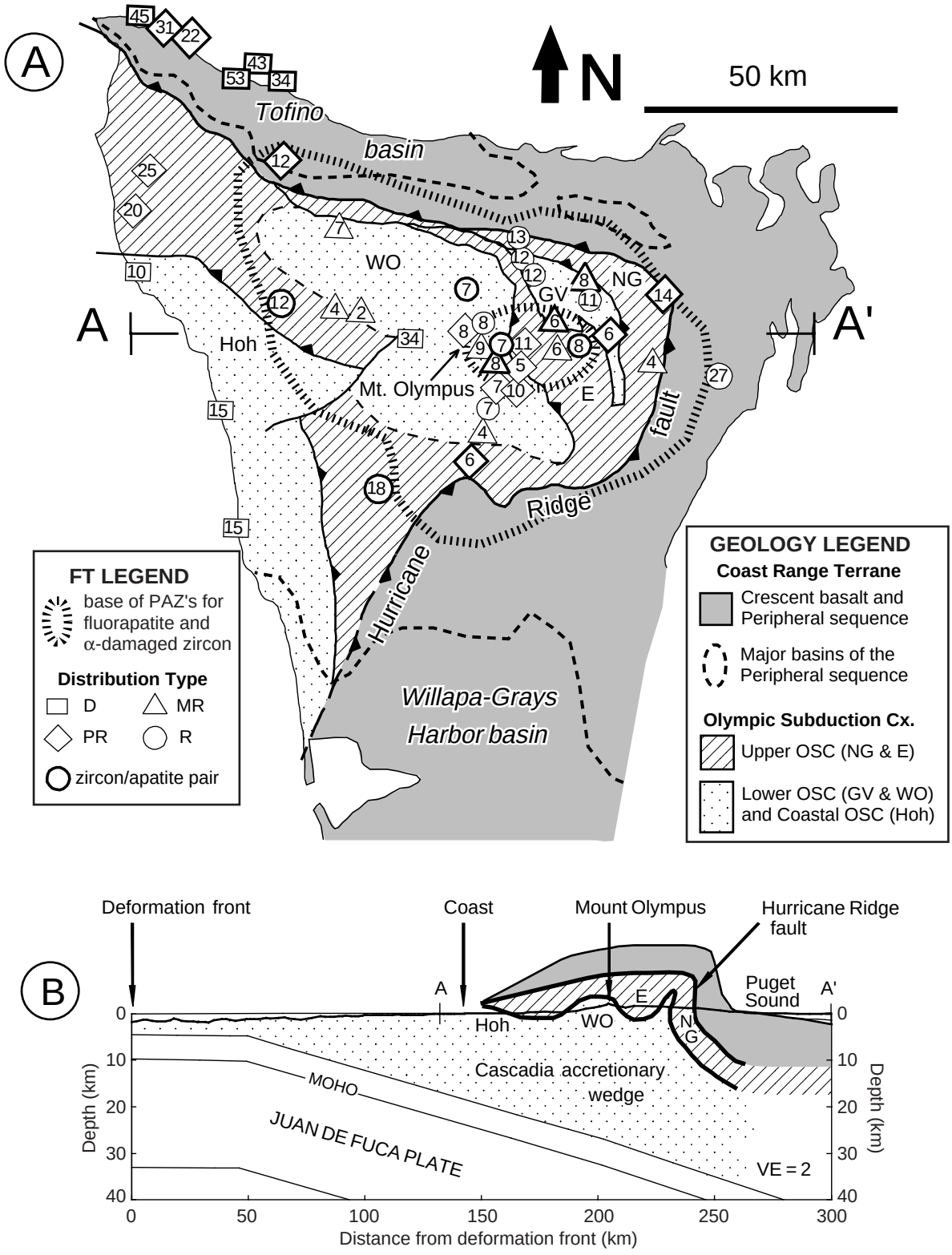

Figure 4. Generalized (A) geologic map and (B) cross section for the Olympic subduction complex (OSC). Numbers indicate minimum ages for apatite fission-track (FT) samples (Tables 1 and 2), and are considered to be reset ages for all MR, PR, or R samples (triangle, diamond, and circle, respectively). Bold outlines indicate localities with published zircon fission-track ages (right sides of Tables 1 and 2). The outer and inner ruled lines mark the base of the partial annealing zone for fluorapatite and α-damaged zircon, respectively. Tectonostratigraphic units of Tabor and Cady (1978a) are shown as NG—Needles–Gray Wolf, E—Elwha, GV—Grand Valley, WO—Western Olympic, and Hoh.

such as the Cascade arc. Thus, the minimum age of the sample, the fission-track age of the youngest fraction of detrital zircons, has proven to be a good proxy for the depositional age of dated Olympic subduction complex sandstones. (An exception is present in the northwest corner of the Olympic Mountains, where local units of the Peripheral sequence—the Makah and Clallam formations—lack young volcanic sediment and give zircon fission-track minimum ages that are significantly older than deposition; see Garver and Brandon, 1994, for details.) Brandon and Vance (1992) reported 11 new depositional ages for the Olympic subduction complex. Work in progress by Richard Stewart (1998, personal commun.) has greatly expanded the number of units and localities dated by the zircon fission-track method, and confirms the general pattern of ages indicated by earlier work.

On the basis of their new zircon fission-track age data and existing geologic mapping, Brandon and Vance (1992) proposed that Tabor and Cady's (1978a) units could be lumped into three regional-scale units called the Upper, Lower, and Coastal units (Figs. 1B and 4).

1. The Upper unit, which includes the Needles–Gray Wolf and Elwha assemblages, is dominated by Eocene clastic sediments, mainly turbidite sandstone and subordinate mudstone. Also present are subordinate lower Eocene pillow basalts, which can be found in depositional contact with the surrounding clastic sediments. The pillow basalts are stratigraphically and compositionally identical to the Crescent basalts exposed in the overlying Coast Range terrane (Tabor and Cady, 1978a; M. Brandon, unpublished data), which implies that the Upper unit is related to the Coast Range terrane.

2. The Lower unit, which includes the Western Olympic and Grand Valley assemblages, is composed solely of clastic sediments, mainly turbidite sandstones. Pillow basalts are notably absent. Zircon fission-track ages indicate that the Lower unit is, at least in part, late Oligocene and early Miocene in age.

3. The Coastal unit of the Olympic subduction complex is equivalent to the Hoh assemblage and consists of turbidites, mudstone, and minor pillow basalt. The sedimentary component of this unit has yielded ~47 fossil localities; most indicate an early and middle? Miocene age (Saucesian and Relizian?; see Rau, 1975, 1979). A few Eocene fossils have been found, some of which come from large isolated blocks of pillow basalt and others from local sedimentary units. The origin of these older rocks remains unclear. Rau (1975, 1979) mapped them as part of the Hoh assemblage, whereas Tabor and Cady (1978a) assigned them to the Western Olympic assemblage. Our own observations indicate that the basalt blocks were probably derived from the overlying Crescent basalts on the basis of similarities in chemistry and internal stratigraphy (M. Brandon, unpublished data). Following Tabor and Cady (1978a), we prefer the interpretation that the Coastal unit is a Miocene accretionary unit that contains local exotic blocks of Eocene basalt and sedimentary rocks. The similarity of the basalt blocks to the Crescent suggests that they may have been produced by submarine landsliding from the overlying Coast Range terrane.

There are important contrasts in deformation and metamorphism between the Coastal unit and the more deeply seated rocks of the Lower and Upper units (Tabor and Cady, 1978a, 1978b; Orange, 1990; Orange et al., 1993; Orange and Underwood, 1995; B. Kang and M. Brandon, unpublished mapping and strain analysis). The Lower and Upper Olympic units were first intensely imbricated and then developed a superimposed pressure-solution cleavage. Mud-rich mélanges are notably rare. Metamorphism is generally prehnite-pumpellyite facies.

In contrast, the Coastal unit generally lacks a cleavage, but otherwise shows a broad range of deformation styles, including thrust-related imbrication, tabular zones of mud-rich mélange, and cylindrical intrusions of mud diapirs. Metamorphic grade is restricted to zeolite facies. Published vitrinite reflectance data indicate a gradual eastward increase in metamorphic temperature across the Coastal unit and into the western part of the Upper unit (Snavely and Kvenvolden, 1989). This pattern appears to hold at the regional scale but it may be complicated at the local scale by out-of-sequence faults, extraformational blocks, and mud diapirism (Orange and Underwood, 1995). Direct comparison of our apatite fission-track ages with published vitrinite results would be useful but is complicated by the presence of local structures and by the fact that available fission-track ages and vitrinite measurements come from different localities. We have recently produced more apatite fission-track results for the Coastal unit, and thus have decided to wait until those data are published before we attempt a detailed comparison between vitrinite and apatite results.

SUMMARY OF TECTONIC EVENTS

The following tectonic synthesis provides an integrated view of the geologic relationships and age data summarized here and a broad context for the following new apatite fission-track data. During latest Eocene time, initiation of a new Cascadia subduction zone caused pervasive imbrication along the west side of the Coast Range terrane. In our view, this event was marked by tens of kilometers of top-W motion on the Hurricane Ridge fault. During this event, the entire lower crust and mantle of the Coast Range terrane were stripped away and subsequently replaced by the highly imbricated Upper unit of the Olympic subduction complex. The Upper unit probably originated as a more westerly extension of the Coast Range terrane and thus would have already been part of the North America plate prior to initiation of subduction. In other words, structural assembly would have occurred by telescoping of the upper plate rather than by accretion from a subducting oceanic plate.

In contrast, the Coastal and Lower units are considered to have originated as abyssal-plain and trench-fill sediments deposited seaward of the Cascadia deformation front. They were accreted to the overriding Cascadia wedge by imbrication along the subduction thrust. The Coastal and Lower units overlap in age, which suggests that their accretion also overlapped in age. The Lower Olympic subduction complex was underplated beneath the wedge at depths of 12 km and greater (Brandon and Vance, 1992), which is consistent with the presence of a pressure-solution cleavage and prehnite-pumpellyite assemblages. In contrast, the lower metamorphic grade and the lack of a cleavage suggest that the Coastal unit was accreted at the front of the wedge by offscraping (Orange et al., 1993).

Miocene stratigraphy provides information about the emergence and subsequent exhumation of the Olympic Mountains uplift. Neritic fossils in the uppermost part of the Peripheral sequence (Astoria?, Clallam, and Blakeley Harbor formations in Fig. 3) indicate that by early Miocene time, the entire area of the Olympic Peninsula had risen to a water depth <200 m (see Armentrout, 1987, for details). Subsequent emergence of the Olympic Mountains is marked by a regional unconformity beneath the middle to upper Miocene Montesano Formation and equivalent unnamed units that underlie the continental shelf west of the Olympic Mountains (Fig. 3). The Montesano Formation itself consists mainly of fluvial deposits derived, in part, from the uplifted Olympic subduction complex and the Coast Range terrane (Tabor and Cady, 1978a, 1978b; Bigelow, 1987). The sub-Montesano unconformity is bracketed stratigraphically by two units of the Columbia River basalts, the Grande Ronde Member (17 to 15.6 Ma) and the Pomona Member (12 Ma) (Armentrout et al., 1983, p. 57; Walsh et al., 1987, p. 12) (see "Southwest" column in Fig. 3). Brandon and Calderwood (1990) stressed the age of the upper flow when they assigned a 12 Ma age to the formation of the unconformity. We now recognize that the unconformity could have formed anytime between 17 and 12 Ma. It is important to note that present exposures of the Montesano unconformity are

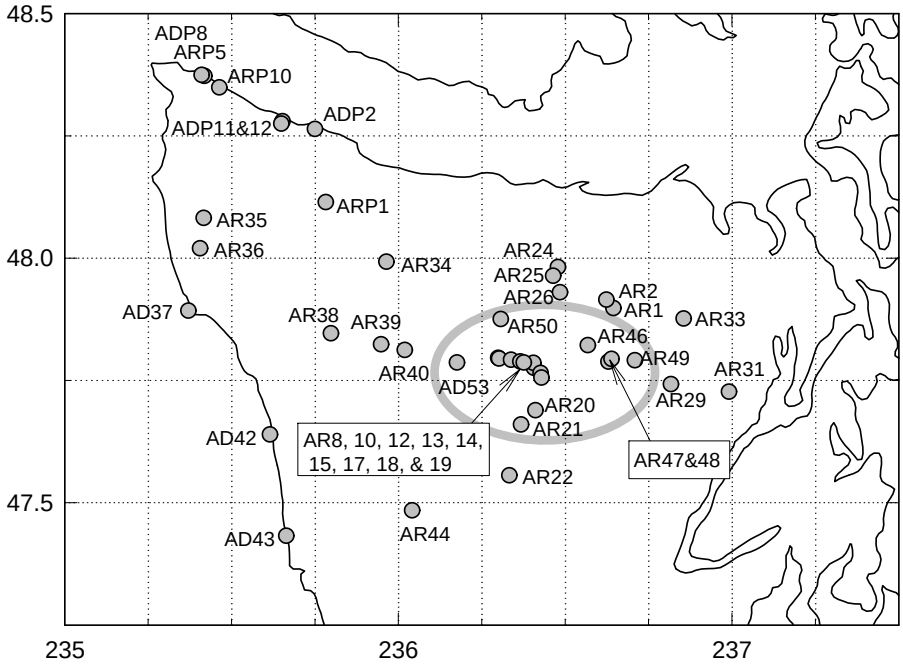

Figure 5. Location map for apatite fission-track samples. Gray ellipse encloses samples from the central massif.

~60 km south of the center of the Olympic Mountains uplift. Emergence may have been diachronous, perhaps occurring first over the center of the Olympic Mountains and then propagating outward with time. The apatite fission-track data presented here provide independent information about the age of emergence for the central and most deeply exhumed part of the uplift.

LABORATORY PROCEDURES

We collected ~2–12 kg samples, typically fine- to medium-grained sandstone, but in one case, a diabasic gabbro from the Crescent Formation. Samples were crushed, washed, and sieved. Apatite was isolated using a Rodgers table, heavy liquids, and magnetic separation. Aliquots (10–20 mg) of apatite were mounted in epoxy on glass slides and polished to expose internal grain surfaces. Mounts were etched for 20 s in 5M HNO_3 at 21 °C. An external detector of low-U muscovite was placed on each mount and secured by tape. Fluence monitors, using the Corning Glass CN1 standard, were placed at each end of the irradiation package. Samples were irradiated with thermal neutrons in a well-thermalized reactor (TRIGA reactor at Oregon State University) using a nominal fluence of ~8×10^{15} n/cm^2. After irradiation, the mica detectors were etched in 40% HF for 15 min. All tracks were counted dry at 1600× using a Leitz Ortholux microscope. Fission-track ages were calculated using a weighted mean zeta calibration factor (Hurford and Green, 1983) based on the Fish Canyon, Durango, and Mount Dromedary apatite standards (Miller et al., 1985). Zeta values with ±1 standard error (SE) are: 103.2 ± 2.3 for M. Roden-Tice and 110.3 ± 2.2 for D. S. Miller. Sample locations are shown in Figures 4 and 5, and fission-track results are in Tables 1 and 2.

THERMAL STABILITY AND CLOSURE OF THE FISSION-TRACK SYSTEM

Modern apatite fission-track analysis relies heavily on track-length data to aid in the interpretation of fission-track ages (e.g., Green et al., 1989; Carlson, 1990). This approach has limited utility when dating detrital apatites, because track-length analysis assumes that all apatites in a sample have the same annealing properties (see Donelick et al., 1998; Ketcham et al., 1998, for an interesting exception). However, heterogeneous annealing is a common feature for apatites from sandstones, and for apatites from some plutonic rocks as well (O'Sullivan and Parrish, 1995). A further problem in our study is that most of our apatites have very few horizontal confined tracks because of low U concentrations and very young fission-track ages. Track-length data are difficult to obtain in any useful quantity. As a result, we are forced to rely on more traditional concepts of a partial-annealing zone and an effective closure temperature, T_c. The following summary provides an updated synthesis of the published literature on fission-track annealing and

Figure 6. Summary of thermal stability and closure temperature (T_c) for fission tracks (FT) in Durango fluorapatite and natural α-damaged zircon. (A) The partial-annealing zones (PAZ) are represented by the 10% and 90% annealing isopleths, which have an Arrhenius-like relationship, $\Delta t = B\, e^{-E/RT}$, where R is the gas constant, T is absolute temperature, E is the activation energy, and B is a proportionality constant. Annealing experiments for Durango fluorapatite (Laslett et al., 1987; Fig. 3 in Green, 1988) indicate E (kcal/mol) and B (m.y.) are 38.07 and 3.117×10^{-26} for 10% annealing, and 46.56 and 1.530×10^{-26} for 90% annealing. Experiments for natural α-damaged zircon (Zaun and Wagner, 1985; Tagami et al., 1990) indicate that E and B are 53.69 and 1.210×10^{-25} for 10% annealing, and 52.76 and 2.552×10^{-22} for 90% annealing. The upward- and downward-facing triangles show published estimates for the limits of the zircon PAZ. Results for the KBT hole at ~100 m.y. (Zaun and Wagner, 1985) were used to estimate the PAZ boundaries. Independent estimates for the zircon PAZ are a contact aureole at ~0.6 m.y. (Tagami and Shimada, 1996) and the Vienna basin hole at ~5 m.y. (Tagami et al., 1996). (B) T_c is estimated for monotonic cooling through the PAZ at an approximately constant cooling rate (see Appendix for details). Symbols show other estimates for T_c: circles = predictions of fluorapatite track-length annealing model ("annealing 3" algorithm of Duddy et al., 1988); triangle—comparison of zircon fission-track ages with apatite fission-track and biotite K/Ar ages (Hurford et al. 1986); squares—comparisons of zircon fission-track ages with $^{40}Ar/^{39}Ar$ K-feldspar ages (Foster et al., 1996); and diamond—comparison of zircon fission-track ages with apatite fission-track and K/Ar biotite ages for the Quattoon pluton (Harrison et al., 1979; note the Harrison et al. result was recalculated using T_c for K-Ar biotite of 300 °C to be consistent with the results of Hurford, 1986). Not included in this summary are experiments of Yamada et al. (1995), which imply anomalously high thermal stability for fission tracks in zircon (see text for discussion). Predictions based on Yamada et al. (1995) would increase T_c for zircon by ~125 °C, 10% annealing by 20 °C, and 90% annealing by 175 °C, relative to our predictions here.

concludes with quantitative estimates for the partial-annealing zone and T_c for fission tracks in fluorapatite and α-damaged zircon.

Dating by the fission-track method is based on spontaneous fission of ^{238}U, which leaves a damage zone in the lattice of many common minerals. The density of fission tracks is related to the production rate of new tracks and the removal of old tracks by thermal annealing. At sufficiently low temperatures, annealing becomes so slow that, for all practical purposes, old and new tracks are fully retained. With increasing temperature, the annealing rate increases until it reaches the point where tracks do not persist for any geologically significant time. The temperature range between these two extremes is known as the partial-annealing zone (p. 123 in Wagner and Van Den Haute, 1992). Strictly speaking, there is no unique partial-annealing zone because the degree of annealing depends on the time-temperature history. However, an idealized partial-annealing zone can be defined by reference to the predicted degree of annealing caused by a stepwise-heating event. T_c is estimated by integrating the effects of track production and annealing for a sample as it cools monotonically through the partial-annealing zone.

Recent research has demonstrated that factors other than mineralogy can affect the thermal stability of fission tracks. For apatite, thermal stability decreases with decreasing Cl content (Green et al., 1985; Crowley et al., 1990, 1991; Carlson, 1990; Donelick et al., 1998). Among the common apatites, fluorapatite has the lowest track stability and T_c, and the best-documented annealing properties. For zircon, thermal stability decreases with increasing α damage (Kasuya and Naeser, 1988). These factors appear to be the most important in controlling the thermal stability of fission tracks in apatite and zircon.

For our analysis, we focus on fluorapatite and α-damaged zircon because they should be the first of their respective mineral group to lose their fission tracks during progressive heating, and the last to start to accumulate tracks during progressive cooling. The estimated partial-annealing zone and T_c for fluorapatite and natural α-damaged zircon are shown in Figure 6. We use the 10% and 90% annealing isopleths to delimit time-temperature conditions for the partial-annealing zone. Our estimates are in reasonable agreement with available data, which include short-term heating in the laboratory and long-term heating in well-characterized boreholes and contact aureoles (see Fig. 6 caption for details). Note that when sustained for >20 m.y., a detectable reduction in the fission-track ages of fluorapatite and α-damaged zircon can occur at relatively modest temperatures, 40 and 175 °C, respectively. Thus, to use the closure temperature concept outlined here, one has to ensure that cooling occurred on a monotonic time-temperature path that moved completely through the partial-annealing zone. When the cooling path gets more complicated, track-length data become essential for the recovery of reliable thermochronologic information.

If a sample cools monotonically through the partial-annealing zone, then track-density data can be used to calculate a meaningful fission-track age. In this case, the age marks the time when the fission-track system closed, but closure is a gradational process given the typical ~60 °C width of the partial-annealing zone. For the simple case of monotonic cooling, one can define T_c as the temperature at the time indicated by the fission-track age equation (Dodson, 1976, 1979). The T_c curves for α-damaged zircon and fluorapatite (Fig. 6B) are estimated using equation 11 in Dodson (1979) and experimental data for 50% annealing during stepwise heating (see details in Appendix). The predictions in Figure 6B are in good agreement with independent estimates of T_c determined from track-length modeling for fluorapatite and comparison of zircon fission-track ages with other isotopic ages (see Fig. 6 caption).

Yamada et al. (1995) and Tagami and Dumitru (1996) argued that the partial-annealing zone and T_c for the zircon fission-track system are about 50 to 100 °C greater than what we have estimated here. We note that their conclusions are based primarily on the Yamada et al. (1995) annealing experiments, which used relatively young (21 Ma) zircons. We suspect that these zircons had a relatively low density of α damage because their fission-track thermal stability is similar to that reported by Kasuya and Naeser (1988) for

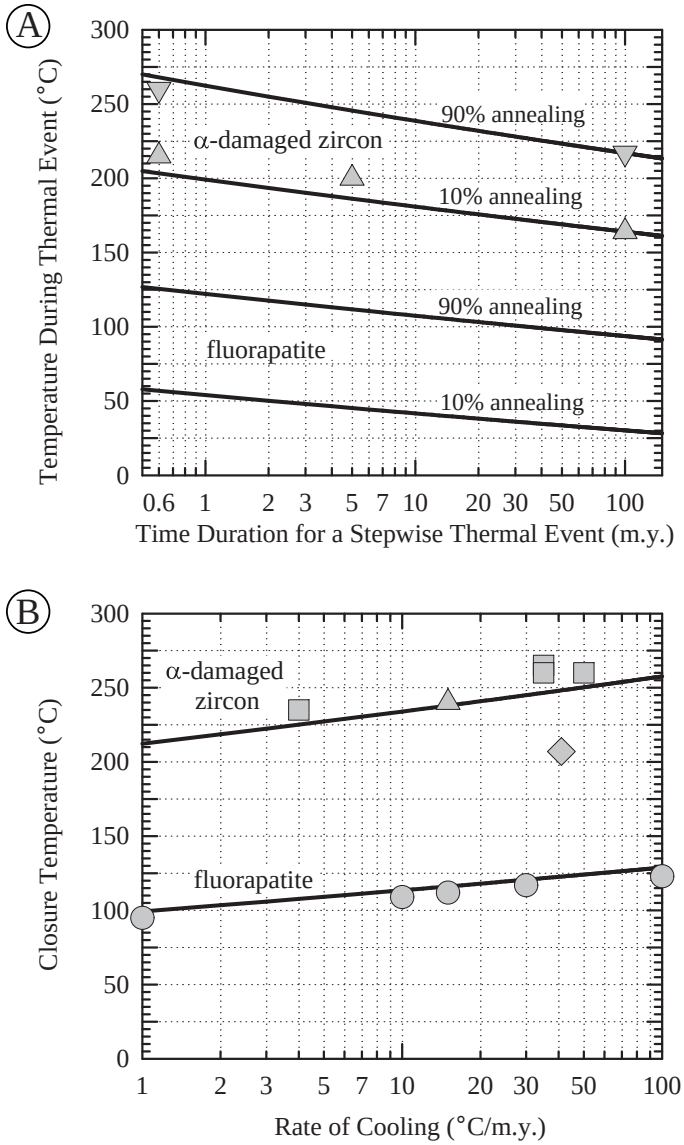

laboratory annealing of induced fission tracks in zircons that had no α damage. Brandon and Vance (1992) showed that thermal resetting had the strongest effect on the oldest fraction of zircons in the Olympic subduction complex sandstones. Their explanation was that those grains had the greatest α damage and were most susceptible to annealing. Given this experience, we infer that the summary for zircon in Figure 6 is most applicable for interpreting the annealing properties of those zircons that had the oldest fission-track grain ages prior to any thermal resetting.

We conclude that Figure 6 provides a reasonable and internally consistent description of the effect of time and temperature on partial annealing and closure for fission tracks in fluorapatite and α-damaged zircon. The similarity between our predictions and other independent estimates (see comparisons in Fig. 6) suggests to us that our estimates of partial-annealing zone and T_c are probably within ±25 °C of the real values, with estimates for fluorapatite being better than those for α-damaged zircon. Note that we cite our temperature estimates to the nearest whole degree, which may give the impression that we are claiming a false level of precision. Our explanation is that much of the uncertainty about temperature estimates is wrapped up in calibrations that affect the entire data set, such as the calibration of apatite and zircon fission-track systems to the temperature scale and the estimation of temperature as a function of depth. Thus, we contend that the internal precision of our temperature estimates are probably better than ±10 °C. In any case, we have also found it useful to report our results to a high precision in order to ensure internal consistency for our various time, temperature, and depth calculations.

Our strategy for dealing with heterogeneous annealing is to use a peak-fitting method (Galbraith, 1988; Galbraith and Green, 1990; Brandon and Vance, 1992; Galbraith and Laslett, 1993) to isolate the youngest group of concordant grain ages. The term "concordant" is used to indicate that the variance of the ages within a group of dated grains is no greater than would be expected from the process of radioactive decay alone. Following Galbraith and Laslett (1993), the fission-track age of the youngest group of concordant grain ages is called the minimum age of the fission-track grain-age distribution. For a sandstone that has always been at temperatures less than the partial-annealing zone, the minimum age corresponds to a young cooling event in the source region of the sandstone. For a sandstone that has been to temperatures within or above the partial-annealing zone, then the minimum age corresponds to the time when the sample cooled to temperatures outside the partial-annealing zone. For apatite fission-track dating, peak-fitting calculations can be supplemented by microprobe analyses to determine the average composition of the youngest grains. This information may help in evaluating the thermal stability of the apatites represented by the minimum age.

ANALYSIS OF FISSION-TRACK RESULTS

Concordant and Discordant Grain-Age Distributions

Current practice uses the χ^2 test (Galbraith, 1981; Green, 1981) to discriminate between concordant [$P(\chi^2)>5\%$] and discordant [$P(\chi^2)<5\%$] grain-age distributions. Note that we have modified this test to account for problems with grains having low spontaneous or induced track counts (N_s and N_i). Grains with N_s or $N_i < 5$ were combined with other grains of similar age so that each observation used in the χ^2 test had N_s and $N_i \geq 5$. This modification reduces the resolution of the χ^2 test, but it also accounts for an essential assumption of the test that N_s and $N_i \geq 5$.

Galbraith and Laslett (1993) argued that their central age gives the best estimate of the average age of the distribution, but they also noted that this age estimate does not have any real meaning for a mixed discordant distribution, defined as a distribution containing two or more grain-age components. In our study, 75% of the samples are mixed discordant distributions. Furthermore, most samples are dominated by young, low-U apatites having low spontaneous track densities. Instead of relying on the central age method, we used the binomial peak-fit method of Galbraith (1988) and Galbraith and Green (1990) to estimate minimum ages and the ages of older components or peaks in the grain-age distribution.[2] Where needed, precise algorithms were used for estimating ages and confidence intervals (for details, see Bardsley, 1983; Sneyd, 1984; Galbraith, 1990; Brandon, 1996). For example, where track counts were low or zero, the exact binomial algorithm of Sneyd (1984) was used to calculate median values and confidence intervals. Confidence intervals were calculated at the 68% and 95% level, which are approximately equal to ±1 SE and ±2 SE, respectively. Uncertainties in the text are cited using a 95% interval, and those in figures and tables are cited using a 68% interval, unless otherwise noted. Note that the confidence intervals for our fission-track ages are generally asymmetric, with the older interval being larger than the younger interval (Tables 1 and 2).

The *F* test was used to determine the number of components in a grain-age distribution (Brandon, 1992). This test addresses the following question: Does the inclusion of an additional component or peak significantly improve the fit of the binomial peak-fit model to the observed fission-track data? The result is reported as a probability *P(F)*. A low *P(F)* indicates that the incremental improvement of the fit is greater than would be expected for random chance alone. The inference is that the added peak is both resolvable and significant.

Interpretation of Discordant Distributions

Results from the binomial peak-fit method are reported in Tables 1 and 2 under "Minimum Age" and "Age of Older Peak." Concordant samples are distinguished by having only one reported age. The remaining discordant samples have no more than two resolvable peaks as determined by the *F* test. The geologic interpretation of these results is based on whether or not the minimum age was reset. As used here, reset means that the youngest concordant group of grain ages was partially or totally annealing during a post-depositional thermal event. This judgement requires knowledge about the depositional age of the sample. Precise paleontological ages would be ideal, but zircon fission-track ages are also useful in this regard. We have already noted that the minimum age for an unreset zircon fission-track sample can be used as a proxy for the depositional age. Alternatively, if the fission tracks in zircons were reset after deposition, then one can assume that fission tracks in fluorapatite were reset as well. Zircon fission-track minimum ages for our samples are listed in Table 1 and 2, an "R" or "D" indicating reset and unreset, respectively, as reported by Brandon and Vance (1992) and Garver and Brandon (1994). Zircon fission-track minimum ages and paleontological ages provide reasonably well constrained estimates of depositional age for about half of our apatite fission-track samples. For the remainder, estimates of depositional age are based on generalized correlations to better dated parts of the Olympic subduction complex.

We have identified four types of apatite fission-track grain-age distributions (Fig. 7). Type R is a single-peak distribution having a peak age younger than the depositional age of the sample. The grains are considered to have been fully reset after deposition and to have acquired a concordant cooling age. Type MR contains more than one peak, but all peaks are

[2]All programs and fission-track (FT) data used in this study are available from the web site: http://love.geology.yale.edu/~brandon. Relevant programs are ZETAAGE (version 4.7), which calculates "exact" FT ages and confidence intervals even for grains with zero fossil tracks, and BINOMFIT (version 1.8), which is an implementation of the binomial peak-fit algorithm of Galbraith (1988). Programs are provided as source code (Quick Basic) and DOS executables.

TABLE 1. APATITE FISSION-TRACK (FT) AGES FOR THE COAST RANGE TERRANE

Lab number	Elevation (m)	Mixture type	χ^2 and *F* tests (%) $P(\chi^2)$	$P(F)$	Minimum age Age	63% C.I.		N_t	Age of older peak Age	63% C.I.		N_t	Stratigraphic age Midpoint	Range	Zircon FT Minimum age
Peripheral sequence (in order of increasing stratigraphic depth)															
ADP2	0	D	0	0	33.5	–2.9	+3.1	13.2	57.6	–3.1	+3.3	35.8	20.9	17.7–24.1	59 D
ADP11	50	D	0	0	42.8	–2.9	+3.1	33.7	63.2	–7.3	+8.2	16.3	26.3	24.1–28.5	64 D
ADP12	100	D	29	72	53.3	–2.4	+2.5	48.0	N.D.	N.D.	N.D.	N.D.	30.6	28.5–32.7	72 D
ARP10	50	PR	1	0	21.7	–4.3	+5.3	2.1	52.8	–3.5	+3.7	17.9	33.4	32.7–34.1	78 D
ARP5	0	PR?	0	0	31.1	–4.1	+4.8	9.4	93.7	–16.1	+19.4	6.6	34.6	34.1–35.0	45 D
ADP8	0	D	0	0	45.0	–6.8	+8.0	6.3	110.9	–15.0	+17.4	13.7	34.6	34.1–35.0	38 D
ARP1	800	PR	0	0	11.8	–1.7	+2.0	6.8	77.7	–15.2	+18.8	3.2	37.7	35.0–40.4	37 D
Crescent basalts															
AR31	91	R	2	100	26.6	–6.4	+8.4	20.0	N.D.	N.D.	N.D.	N.D.	54	N.D.	N.D.

Notes: Mixture types: R = single peak younger than deposition, MR = multiple peaks all younger than deposition, PR = multiple peaks with at least one peak younger than deposition, D = multiple peaks with all peaks older than deposition. $P(\chi^2) = \chi^2$ probability for concordance of grain ages. Minimum ages and older peak ages were calculated using the binomial peak-fit method (Galbraith and Green, 1990). P(F) = probability that the improvement of fit associated with inclusion of an older peak in the peak-fit model could be due to random chance alone. P(F) > 5% is considered to indicate a concordant single-peak distribution. The estimated 63% confidence interval (C.I.), which is approximately equal to $\pm 1\sigma$, was calculated using precise algorithms (see Brandon, 1996, for details). N_f = number of grain ages in peak. The sum of N_f for the fitted peaks is forced to equal the total number of grains. Stratigraphic ages and zircon FT ages are from Garver and Brandon (1994). The zircon FT minimum age correspond to the youngest peak age for detrital zircons dated from the same sample. The suffix "D" indicates that the zircon FT grain-age distribution is unreset and preserves pre-depositional ages. N.D. = not determined.

TABLE 2. APATITE FISSION-TRACK (FT) AGES FOR THE OLYMPIC SUBDUCTION COMPLEX

Lab number	Elevation (m)	Mixture Type	χ^2 and F tests (%) $P(\chi^2)$	P(F)	Minimum age Age	63% C.I.		N_f	Age of older peak Age	63% C.I.		N_f	Central age Age	63% C.I.		N_t	Zircon FT Minimum age
Central massif area (in order of increasing elevation)																	
AR21	399	MR	1	0	4.4	–1.2	+1.6	7.8	16.6	–5.9	+9.2	6.2	8.1	–1.6	+2.6	14	N.D.
AR50	408	R	19	100	6.8	–1.5	+1.8	12.0	N.D.	N.D.	N.D.	N.D.	6.8	–1.4	+2.0	12	27 D
AR20	611	R	10	12	6.8	–1.2	+1.5	13.0	N.D.	N.D.	N.D.	N.D.	6.9	–1.2	+1.6	13	N.D.
AR19	865	PR	0	0	9.9	–1.5	+1.8	14.0	108	–30.0	+41.4	2.0	17.5	–4.2	+7.8	16	N.D.
AR46	945	MR	2	8	5.5	–2.2	+3.6	5.8	10.9	–3.6	+5.5	6.2	7.9	–1.3	+1.9	12	13.1 R
AR12	1021	PR	0	0	5.1	–2.0	+3.2	3.2	32.8	–9.3	+12.9	6.8	21.9	–5.0	+9.4	10	N.D.
AR18	1149	PR	0	0	10.7	–2.7	+3.6	7.1	68.2	–15.7	+20.3	5.9	32.9	–7.0	+12.1	13	N.D.
AR17	1439	R	12	87	7.1	–1.4	+1.8	17.0	N.D.	N.D.	N.D.	N.D.	7.2	–1.4	+1.9	17	14.3 R
AR10	1482	PR	5	0	7.0	–1.5	+1.8	9.6	59.7	–28.8	+55.4	1.4	8.1	–1.4	+2.0	11	N.D.
AD53	1585	D	0	52	33.9	–5.0	+5.9	27.0	N.D.	N.D.	N.D.	N.D.	33.9	–4.6	+6.2	27	N.D.
AR47	1723	MR	0	0	5.7	–2.2	+3.6	10.9	11.7	–4.4	+6.9	9.1	8.3	–1.2	+1.6	20	N.D.
AR8	1771	MR	0	0	8.3	–1.4	+1.7	13.5	16.6	–2.9	+3.5	6.5	11.1	–1.2	+1.4	20	14.4 R
AR15	1845	R	24	100	7.7	–1.1	+1.3	22.0	N.D.	N.D.	N.D.	N.D.	7.7	–1.1	+1.4	22	N.D.
AR48	1982	R	51	100	7.6	–1.2	+1.4	10.0	N.D.	N.D.	N.D.	N.D.	7.6	–1.2	+1.4	10	14.5 R
AR14	2058	MR	0	6	9.0	–2.6	+3.7	12.1	13.9	–7.5	+16.3	11.9	11.4	–1.3	+1.8	24	N.D.
AR49	2060	PR	0	0	6.4	–1.3	+1.7	11.0	17.5	–7.1	+11.9	4.0	8.5	–1.2	+1.8	15	19 D
AR13	2418	PR	0	0	7.5	–0.9	+1.0	24.8	55.3	–19.6	+30.2	2.2	11.2	–1.8	+2.8	27	N.D.
Perimeter area (in order of increasing elevation)																	
AD42	0	D	5	0	15.2	–2.5	+3.0	12.7	23.8	–6.6	+9.1	7.3	18.2	–1.6	+1.8	20	N.D.
AD43	0	D	0	0	15.4	–1.6	+1.8	17.0	41.1	–12.2	+17.3	2.0	17.2	–1.7	+2.1	19	N.D.
AD37	0	D	0	0	10.1	–2.7	+3.7	10.6	23.5	–4.3	+5.3	9.4	16.6	–2.2	+3.0	20	N.D.
AR36	125	PR	0	0	20.3	–2.2	+2.4	15.2	47.8	–12.2	+16.3	4.8	25.9	–2.7	+3.4	20	N.D.
AR22	155	PR	10	0	6.0	–1.8	+2.6	14.6	36.8	–20.0	+43.6	1.4	8.0	–1.8	+2.7	16	32 D
AR44	183	R	7	45	18.4	–2.8	+3.3	9.0	N.D.	N.D.	N.D.	N.D.	18.5	–2.8	+3.5	9	48 D
AR35	198	PR	2	0	24.6	–2.6	+2.9	17.0	46.3	–13.9	+19.8	3.0	27.1	–2.4	+2.8	20	N.D.
AR39	293	MR	0	0	3.9	–0.8	+1.1	15.9	10.1	–1.8	+2.1	15.1	6.8	–0.8	+1.0	31	N.D.
AR40	369	MR	0	3	2.3	–0.9	+1.5	5.1	6.1	–2.2	+3.5	6.9	4.1	–0.8	+1.2	12	N.D.
AR38	508	R	3	100	11.7	–1.7	+2.1	20.0	N.D.	N.D.	N.D.	N.D.	11.7	–1.6	+2.2	20	47 D
AR26	512	R	5	42	11.5	–1.2	+1.3	18.0	N.D.	N.D.	N.D.	N.D.	11.5	–1.1	+1.4	18	N.D.
AR29	534	MR	0	0	4.3	–1.4	+2.1	9.3	15.9	–3.1	+3.9	12.7	10.5	–1.6	+2.2	22	N.D.
AR25	890	R	67	100	12.4	–1.1	+1.2	20.0	N.D.	N.D.	N.D.	N.D.	12.4	–1.0	+1.2	20	N.D.
AR33	939	PR	0	0	13.9	–2.0	+2.3	10.9	61.8	–16.2	+21.9	2.1	20.1	–3.6	+5.4	13	38 D
AR34	945	MR	0	0	6.8	–2.1	+3.1	3.9	16.1	–2.3	+2.6	16.1	14.1	–1.6	+2.2	20	N.D.
AR24	1524	R	21	28	12.6	–1.1	+1.2	19.0	N.D.	N.D.	N.D.	N.D.	12.6	–1.0	+1.3	19	N.D.
AR1	1745	R	5	100	11.4	–1.9	+2.2	15.0	N.D.	N.D.	N.D.	N.D.	11.4	–1.8	+2.4	15	N.D.
AR2	1920	MR	1	2	8.0	–2.9	+4.5	7.1	14.2	–3.2	+4.2	12.9	11.8	–1.4	+1.8	20	34 D

Notes: See notes in Table 1 for general explanation. Central age is calculated according to Galbraith and Laslett (1993). N_t is the total number of dated grains. Zircon FT minimum ages are the youngest peak ages from Brandon and Vance (1992), and the suffix indicates type of age: R = cooling age for reset zircons; D = detrital ages for unreset zircons. Paired apatite/zircon ages come from the same sample except for apatite sample AR8 which is paired with a nearby reset zircon sample ZR9 collected at 1665 m elevation. N.D. = not determined.

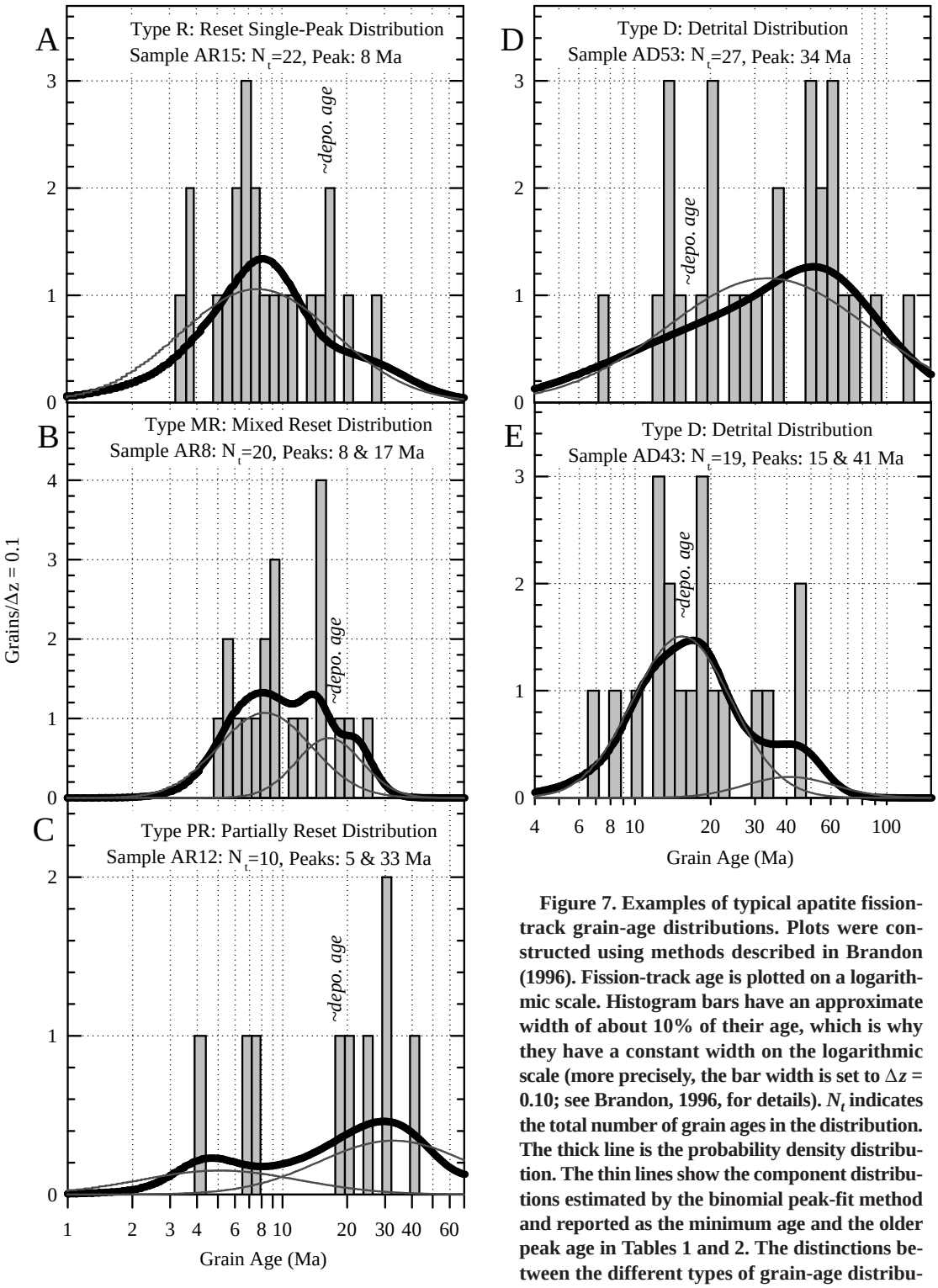

Figure 7. Examples of typical apatite fission-track grain-age distributions. Plots were constructed using methods described in Brandon (1996). Fission-track age is plotted on a logarithmic scale. Histogram bars have an approximate width of about 10% of their age, which is why they have a constant width on the logarithmic scale (more precisely, the bar width is set to Δz = 0.10; see Brandon, 1996, for details). N_t indicates the total number of grain ages in the distribution. The thick line is the probability density distribution. The thin lines show the component distributions estimated by the binomial peak-fit method and reported as the minimum age and the older peak age in Tables 1 and 2. The distinctions between the different types of grain-age distributions are based on the relationship between the minimum age and depositional age of the sample (see text for details).

younger than deposition. The grain ages were reset but are otherwise discordant. Type PR contains multiple peaks, some younger and others older than deposition. The inference is that only a fraction of the grain ages were reset. Type D is distinguished by the fact that all resolvable peaks in the distribution are older than deposition and thus the grain ages are inherited from the source region. For this case, the degree of discordance depends on the fission-track ages of the source region.

In distinguishing a distribution type, we focus on peak ages because individual grain ages typically have very low precision (relative standard errors of ~30% and greater are common for apatite). To illustrate, consider sample AD53 (Fig. 7D), which has some apatite fission-track grain ages that are nominally much younger than the sample's Miocene depositional age. Nonetheless, the distribution has only one resolvable peak at $33.9^{+3.6}_{-3.2}$ Ma (Table 2), which is significantly older than deposition. Sample AD43 (Fig. 7E) has a significant number of apatites younger than its deposition age (about 18 Ma), but its youngest peak age, $15.4^{+3.6}_{-3.2}$ Ma, is not significantly younger than deposition. Young grain ages are expected for type D samples because much of the sediment in the Olympic subduction complex was derived from the active Cascade volcanic arc (Brandon and Vance, 1992).

A useful test of our peak-fitting analysis is to see if we can resolve a correlation between elevation and fission-track age, which is expected in areas of large topographic relief (e.g., Wagner et al., 1977). Figure 8A shows central ages versus elevation for the various reset samples from the Olympic subduction complex (types R, MR, and PR). Ages for concordant samples [solid symbols; $P(\chi^2)>5\%$] show a steep trend with elevation, but ages for discordant samples [open symbols; $P(\chi^2)<5\%$] are on the old side of this trend. Figure 8B shows the same reset samples but now using their minimum ages. For this case, the steep trend is well defined by both concordant and discordant samples. This result supports our inference that the youngest concordant group of grain ages in the R, MR, and PR samples all have similar annealing properties and thus underwent fission-track closure at the same temperature. The three ages off the trend are for localities west of the Olympic uplift (AR35, AR36, AR44). Their older ages are attributed to slower exhumation in the flanks of the uplift.

This exercise illustrates a well-known point: concordance or discordance of a fission-track grain-age distribution is not sufficient by itself to determine if the distribution was reset after deposition. Discordance in an unreset sandstone is likely given that a typical source region will have a heterogeneous cooling history. Discordance in MR or PR samples, where a significant fraction of the grain ages have been reset to an age younger than deposition, is commonly attributed to heterogeneous annealing.

We examined the correlation of Cl content with fission-track age by analyzing a subset of the dated apatite grains (Fig. 9). The gray lines show minimum ages and older peak ages from Table 2. The best example of compositional control on annealing is sample AD53 (Fig. 9A), which has grains with relatively old ages and relatively high Cl contents (19% chlorapatite). For comparison, Durango apatite has 5% chlorapatite, and the most chlorine-rich apatites from the Otway basin are 20% to 30% chlorapatite (Green et al., 1985, Fig. 5). Sample AD53 comes from the central part of the Olympic uplift. It has only one peak having an age of 34 Ma, whereas other nearby apatite localities have reset youngest peak ages that cluster between 2 and 9 Ma (Fig. 4A).

The relationship between Cl content and grain age is not so clear for the MR and PR samples in Figure 9. Cl-rich apatites are rare among the analyzed grains. Furthermore, the old peak in each distribution appears to have more F-rich than Cl-rich apatites. The data do indicate, however, that the youngest fraction of grain ages in the type R, MR and PR distributions are dominated by fluorapatites. Thus, the time-temperature relationships summarized in Figure 6 should be appropriate for interpreting fission-track minimum ages for our apatite samples.

Although we believe that we have a good strategy for interpreting our data, we remain puzzled about the factors contributing to grain-age discordance within our reset samples. The microprobe data suggest that something other than Fl/Cl composition is involved. To illustrate the problem, consider the MR samples, for which all grains were reset to ages younger than deposition, but the age distribution remains discordant. From Table 2, we calculate that the difference between

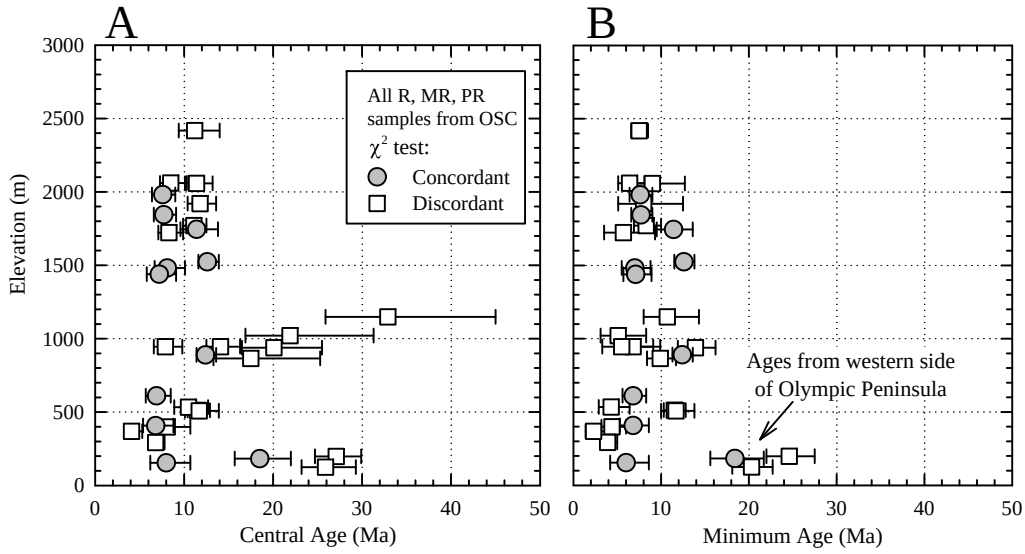

Figure 8. Age-elevation relationship for reset apatite fission-track ages from the Olympic subduction complex (OSC) (type R, MR, and PR samples in Table 2). The two plots show the relative performance of (A) central ages and (B) minimum ages. Error brackets are at the 68% confidence interval.

the minimum age and older peak age in an MR sample averages ~7.4 m.y.; the range is from 3.8 to 12.2 m.y. One explanation is that the difference in age is related to two populations of grains that have different closure temperatures, T_c. Using results given below for the thermal gradient ~19 °C/km, and the average exhumation rate ~0.75 km/m.y., we estimate that the difference in T_c would have to be about 100 °C, which seems much too large to be reasonable.

A second explanation is that the apatites associated with the older peak were never totally annealed and thus retain "old" tracks. This explanation also requires a very high thermal stability for the "old" apatites, given that some of the MR samples come from the reset zircon zone in the central part of the uplift (Fig. 4). For example, sample AR8 has a minimum age of 8 Ma and an older peak age of 17 Ma, whereas reset zircons give a fission-track minimum age of 14 Ma. Correlation with other parts of the Lower unit of the Olympic subduction complex suggest deposition of this sample before 19 Ma, probably during early Miocene or late Oligocene time. Maximum temperatures are estimated to have been >240 °C (Brandon and Vance, 1992), well in excess of temperatures considered necessary to anneal apatites.

A third explanation for the discordance is that U was leached out of some of the apatites after fission-track closure, which would result in relatively old fission-track grain ages. This possibility is suggested by the fact that many of the apatites in our study showed corroded external shapes, suggesting dissolution by a fluid phase. Work in progress has produced more apatite

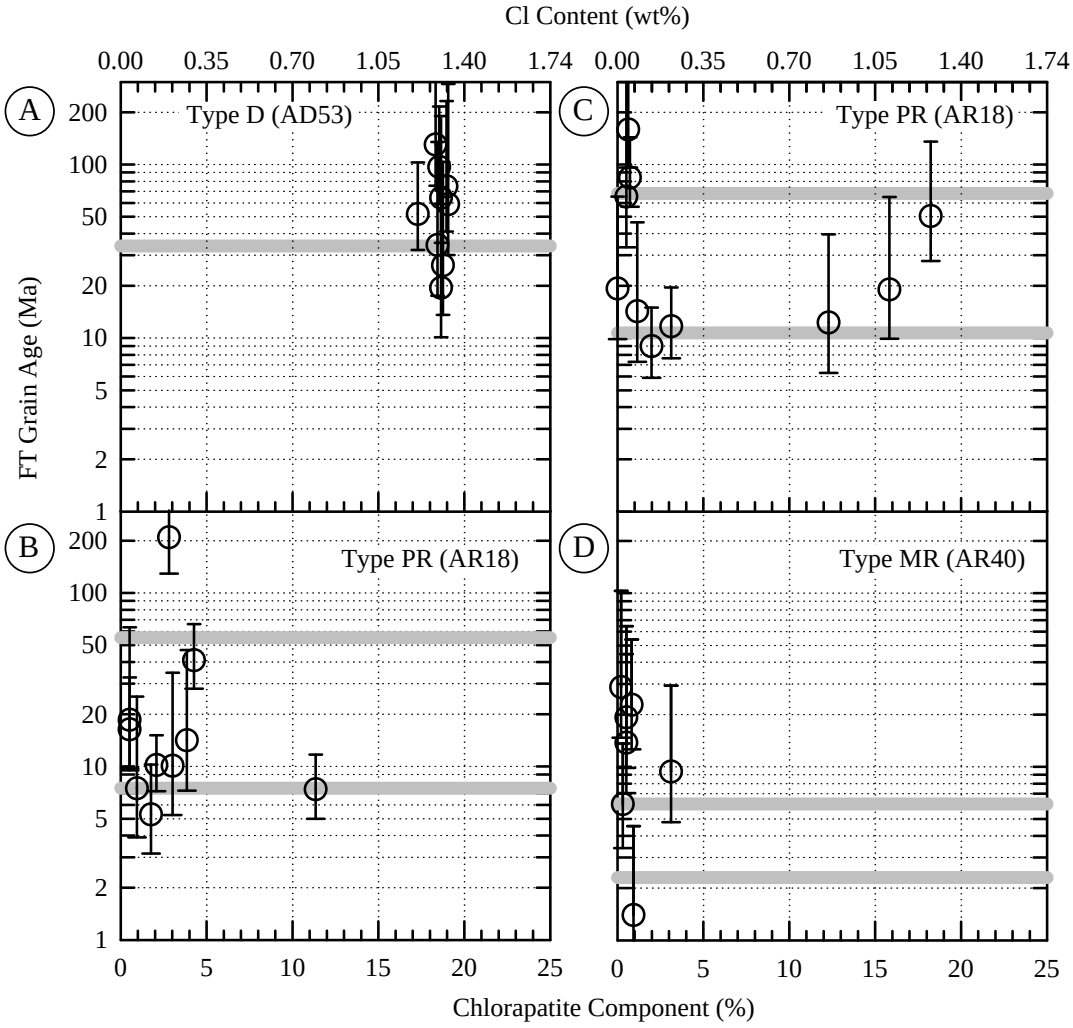

Figure 9. Comparison of fission-track (FT) ages with Cl content for individual apatite grains. Peak ages from Table 2 are shown by the horizontal gray lines. Apatite composition was determined on a JEOL 733 Superprobe with a 15 kv accelerating potential, 13 nA sample current, and a 15 μm beam diameter. Natural and synthetic glasses and minerals were used for standards. Data reduction was by the Bence and Albee (1968) method. Chlorapatite composition (bottom axis) is the percentage of chlorine atoms filling anion sites in apatite. Grain ages and uncertainties were calculated using exact algorithms for a binomial distribution (Sneyd, 1984; Bardsley, 1983). Uncertainties correspond to the 68% confidence interval. Grains with low track counts are assigned an estimated median age (confidence probability of 50%), which explains why there are no "zero age" grains. Note that the median age converges with the mean age as the induced and spontaneous track counts increase (see Brandon, 1996, for details). Grain ages are plotted on a logarithmic scale to show details in the vicinity of the expected closure age (ca. 15 to 2 Ma). See text for further discussion.

fission-track data for areas around the perimeter of the Olympic uplift. Those apatites tend to preserve more euhedral shapes and generally give concordant fission-track results, which supports the idea that dissolution might be contributing to discordance.

At present, we do not favor any single explanation for the discordance in the MR and PR samples. All of the possibilities outlined here could be involved. More important, however, is the conclusion that the problem of discordance seems to have no significant influence on the minimum ages of our apatite samples.

GEOLOGIC INTERPRETATION OF FISSION-TRACK RESULTS

We focus here on the following topics: (1) the initial thermal structure of the forearc high prior to the onset of uplift and exhumation, as recorded in the Coast Range terrane; (2) the detailed exhumation history of the central massif; and (3) the regional pattern of exhumation across the entire Olympic Peninsula. The fission-track data are organized into three groups. Table 1 reports the Coast Range group; samples are shown in order of increasing stratigraphic depth. Table 2 reports the Olympic subduction complex samples, which are separated into a central massif group (circled by gray ellipse in Fig. 5) from the core of the Olympic Mountains where elevation, relief, and exhumation are greatest, and a perimeter group from surrounding lowland areas. The Olympic subduction complex samples are ordered according to elevation.

Coast Range Terrane

The eight youngest peak ages from the Coast Range terrane show evidence of progressive resetting with increasing stratigraphic burial (Fig. 10). The three shallowest samples show no resetting. All have type D distributions; all peak ages are significantly older than deposition. The next three samples have type PR or D distributions, indicating variably resetting within the apatite partial-annealing zone. The stratigraphically highest sample of this group, ARP10, has a ca. 22 Ma minimum age, which is younger than the its depositional age (about 33 Ma). The middle sample of the group, ARP5, has a minimum age that is indistinguishable from its depositional age. The lowest sample, ADP8, has not been reset given that its minimum age is older than deposition. All samples below this stratigraphic level are clearly reset. For example, ARP1 has a reset minimum age of 12 Ma, relative to its depositional age of 38 Ma. AR31, a diabase from the lower part of the Crescent Formation, gives a concordant reset age of 27 Ma, which is much younger than the ca. 54 Ma igneous age of the Crescent Formation (Duncan, 1982). Note that the Olympic subduction complex samples that structurally underlie these Coast Range terrane localities are also clearly reset, and have minimum ages between 14 and 4 Ma (Fig. 4A).

These data suggest that prior to ca. 12 Ma, the base of the fluorapatite partial-annealing zone was located between samples ADP8 and ARP1 at 4.7 ± 0.9 km depth. The three samples within the inferred partial-annealing zone show erratic apparent ages, which is typical for detrital apatites that have never been below the apatite partial-annealing zone. The 6-km-thick section of the Peripheral sequence that we sampled was deposited between about 40 and 20 Ma and was uplifted and eroded between 20 to 10 Ma (see depositional age versus depth in Fig. 10). This burial-erosional history indicates that the base of Peripheral sequence was at maximum temperatures for ~20 m.y. Figure 6A indicates that a temperature of ~100 °C would be required to cause 90% annealing in fluorapatites in 20 m.y. Thus, prior to uplift and exhumation, the temperature and depth at the base of the fluorapatite partial-annealing zone is estimated to have been ~100 °C and ~4.7 km. Assuming an average surface temperature of ~8 °C, which is the modern value, we estimate that the pre-exhumation thermal gradient in the Olympic Mountains was 19.5 ± 4 °C/km. This result is similar to the modern thermal gradient along strike in other parts of the Cascadia forearc high (19.4 ± 1.7 °C/km; see Brandon and Vance, 1992, for details).

Sample ARP1 is a particularly sensitive indicator of the onset of uplift and exhumation because the sample was located just below the base of the partial-annealing zone. Thus, we consider the 12 Ma reset minimum age for this sample to indicate the start of exhumation in this part of the Olympic Peninsula. This interpretation may seem to conflict with the stratigraphically deeper sample AR31, which indicates fission-track closure at 27 Ma, but this age has a very large uncertainty (95% confidence interval is 14 to 43 Ma) and thus is not useful for constraining the timing of exhumation.

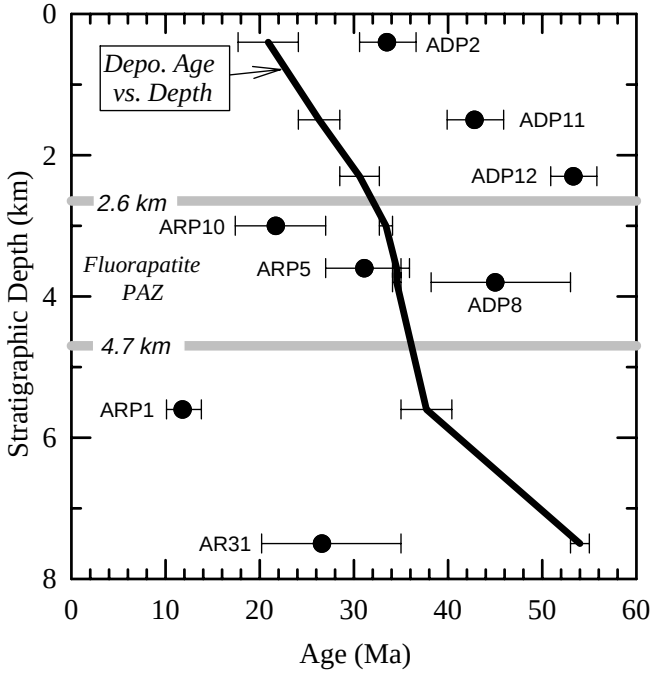

Figure 10. Apatite fission-track minimum ages as a function of stratigraphic depth in the Coast Range terrane. The solid line shows deposition (Depo.) age versus stratigraphic depth; error brackets show the permissible depositional age range for each sample. Apatite fission-track minimum ages are shown by solid circles; error brackets indicate the 68% confidence interval. All samples, except for the lowest, are from a section through the Peripheral sequence in the northwest corner of the Olympic Peninsula (Tofino basin in Fig. 4). The lowest sample, AR31 from a diabase dike in the Crescent Formation, was collected on the east side of the Olympic Peninsula. Stratigraphy and depositional ages are from Snavely et al. (1980), Duncan (1982), Armentrout et al. (1983, 1988), and Garver and Brandon (1994). *PAZ*—partial annealing zone.

Olympic Subduction Complex

Of the 35 apatite samples from the Olympic

subduction complex (Table 2), 31% have R distributions, 29% have MR distributions, 29% have PR distributions, and 11% have D distributions. The distribution types show no obvious pattern in map view (Fig. 4A).

A spatial pattern is obvious for the reset minimum ages (Fig. 4A); the minimum ages are youngest in the central massif and gradually increase outward to the coast. This pattern correlates with the modern topography of the peninsula. Almost all of the reset minimum ages are middle Miocene age and younger, compatible with the stratigraphic evidence (Fig. 3) for exhumation of the Olympic Mountains starting in middle Miocene time. Three cooling ages are older than middle Miocene (20, 25, and 18 Ma for samples AR36, AR35, AR44), but they come from the western flank of the Olympic uplift, and are considered to have always been above the base of the fluorapatite partial-annealing zone (discussed below). If correct, these fission-track ages would not have any direct thermochronologic significance.

Correlation Between Fission-track Age and Elevation for the Central Massif

Both zircon and apatite fission-track minimum ages from the central massif show well-defined linear trends when plotted against elevation (Fig. 11). The slope of the regression line can provide a direct estimate of the long-term exhumation rate, but only if the closure isotherms for these fission-track ages remained fairly flat and stationary relative to the Earth's surface during cooling (Stüwe et al., 1994). However, we know that the onset of exhumation will cause the closure isotherm to migrate toward a new steady-state configuration. The measured exhumation rate will be reduced relative to its true value by an amount equal to the upward velocity of the closure isotherm at the time that the sample moved through the isotherm. For the Olympic Mountains, we estimate that the upward velocity of the closure isotherms dropped to <20% of the true exhumation rate within 3 to 4 m.y. after the onset of exhumation (Appendix Fig. A2). Thus, the zircon fission-track ages, which closed shortly after the onset of uplift and exhumation, might give a low estimate of the exhumation rate, but the apatite fission-track ages, which closed at ca. 7 Ma, should not be significantly affected by this transient.

A second problem with the age-elevation relationship is that isothermal surfaces can become distorted in the presence of large topographic relief and fast exhumation rates. The analysis of Stüwe et al. (1994) indicates that this effect is not important for the Olympic Mountains given the relatively low topographic relief (~1 km), modest exhumation rates (~1 km/m.y.), and low initial thermal gradient (~19 °C/km).

Regression lines were fit to the data using weighted least squares (see Fig. 11 for details). This analysis indicates that a sample from the current local mean elevation of the central massif (1204 m) would have passed through the α-damaged zircon T_c at 13.7 Ma at a rate of 0.76 km/m.y. (±2 SE: 0.43 to 3.0 km/m.y.) and through the fluorapatite T_c at 6.7 Ma at a rate of 1.2 km/m.y. (±2SE: 0.58 to ∞ km/m.y.).

Exhumation History of the Central Massif

The shape of the time-temperature-depth path can be constrained at four points: (1) initial accretion at the base of the wedge, (2) closure for α-damaged zircon fission-track ages, (3) closure for fluorapatite fission-track ages, and (4) present exposure at the Earth's surface. These data points are summarized here, with a specific focus on the relationship between exhumation, closure temperature, and the evolving thermal structure of the wedge. Our interpretation is summarized in Figure 12. The thick line shows the path for a point currently at the mean elevation of the central massif. The dotted lines mark the paths of the lowest ("V") and highest ("S") points in the topography, corresponding to sea level and the 2417 m summit of Mount Olympus, respectively. Depth is always with respect to contemporaneous local mean elevation.

The Lower unit of the Olympic subduction complex, which is the main unit exposed in the central massif, is inferred to have been deposited in the trench seaward of the Cascadia subduction zone during late Oligocene and early Miocene time (~27 to 19 Ma) (Brandon and Vance, 1992). Accretion of the Lower unit would have occurred within ~2 m.y. after deposition, given typical convergence rates (normal component of convergent has been ~40 to 50 km/m.y. over the past 37 m.y.; see Engebretson et al., 1985, p. 71). The maximum depth of accretion can be inferred from the reset zircons in the center of the uplift. The inner ruled line in Figure 4A encloses the area within the central massif where α-damaged zircons were fully reset. We infer that rocks within the reset zone were subducted to depths and temperatures that exceeded the base of the α-damaged zircon partial-annealing zone. Brandon and Vance (1992) found that the transition from unreset to reset zircons currently occupies a

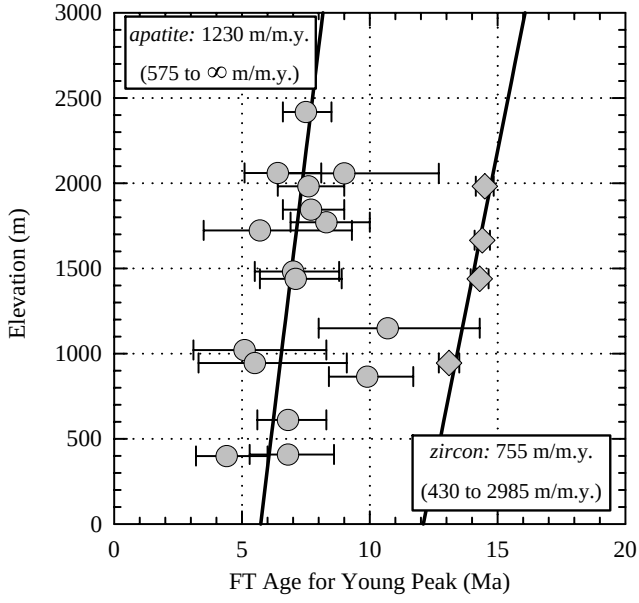

Figure 11. Age-elevation plot of fission-track (FT) minimum ages for apatite and zircon samples from the central massif. Error brackets ages show the 68% confidence interval. Regression lines were fit using weighted least squares (Press et al., 1992, p. 655–660). Errors were assumed to reside totally in the fission-track ages and weights were assigned using the age uncertainties. The estimated exhumation rate is equal to the inverse of the slope of the regression line and its uncertainty is calculated from the uncertainty for the estimated regression slope (Press et al., 1992, p. 657). This accounts for the asymmetric uncertainties for the estimated exhumation rates, the upper interval being much larger than the lower interval. Note that if the error brackets for the individual ages were extended to the 95% confidence interval, they would all overlap their respective best-fit line.

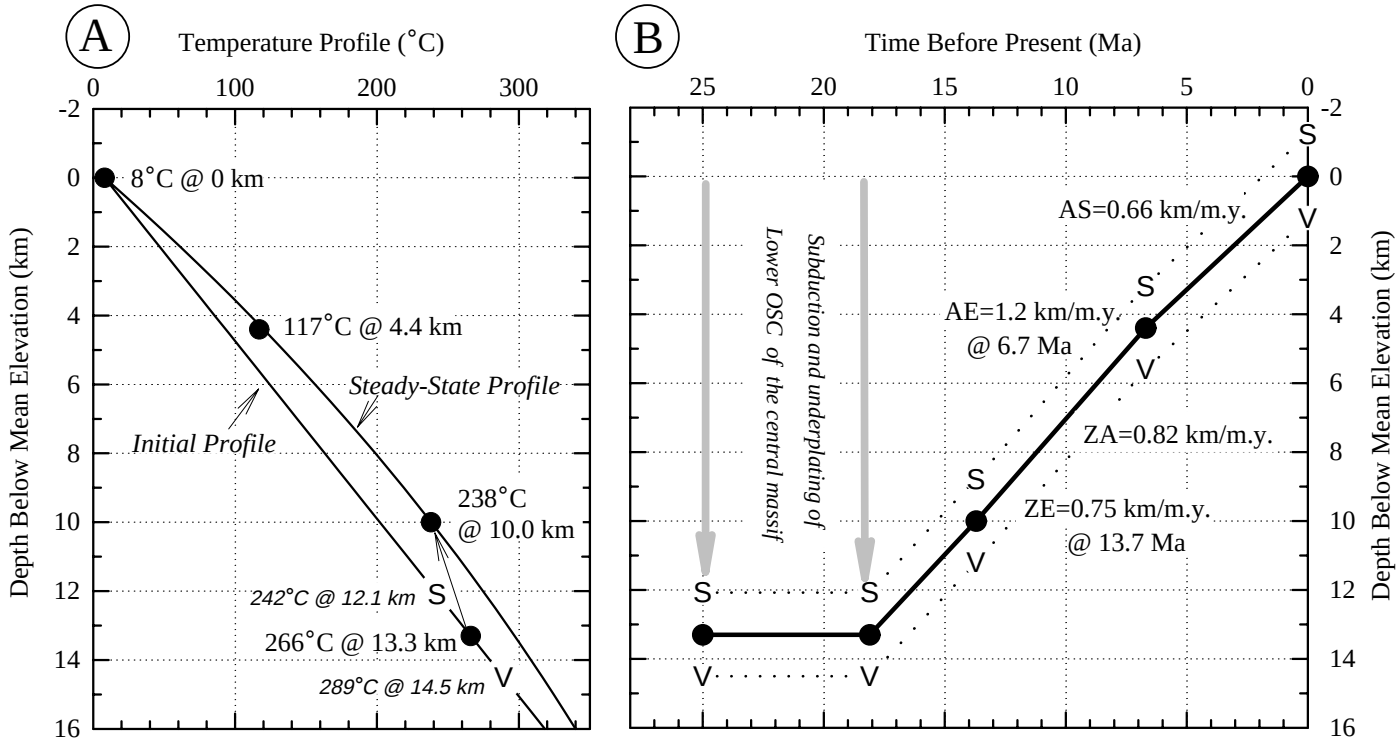

Figure 12. Thermal and exhumation history of the central massif. OSC—Olympic subduction complex. All depths are referenced to mean elevation of the central massif (1204 m). V and S indicate points that currently are at sea level and at the summit of Mount Olympus (2417 m), respectively. (A) Initial profile is the estimated geotherm before exhumation. Steady-state profile is the predicted geotherm for a steady exhumation rate in the range 0.65 and 0.85 km/m.y. V and S on the initial profile show the initial depth and temperature for rocks currently exposed in the central massif. Exhumation caused rocks to move upward along a path close to the steady-state profile. Points along the depth-temperature curve (solid circles) show the starting depth and closure depths for α-damaged zircon and fluorapatite for rocks currently at local mean elevation in the central massif. (B) Exhumation path for points that currently are at local mean elevation (heavy line), sea level (dotted line with V's), and the Mount Olympus summit (dotted line with S's). ZE and AE indicate exhumation rates determined from the age-elevation plot (Fig. 11) for α-damaged zircon and fluorapatite, respectively. ZA and AS indicate exhumation rates estimated for times between α = damaged zircon and fluorapatite closure and fluorapatite closure and surface exposure, respectively.

map distance of only 5 to 10 km, which suggests that the fossil partial-annealing zone was folded into a domal antiform around the central reset area. The domal structure is indicated because all samples within the inner ruled line in Figure 4A, including ones from the highest summits (up to 1982 m; Fig. 11), were subject to temperatures that could have fully annealed α-damaged zircons. Timing constraints indicate that the time available for thermal resetting was ~5 m.y., and probably no more than 10 m.y., which indicates that the temperature at the base of the α-damaged zircon partial-annealing zone was ~240 to 245 °C (Fig. 6A). In Figure 12A, the highest summits in the Olympic Mountains are considered to have been just below the base of the α-damaged zircon partial-annealing zone just prior to the onset of exhumation; thus they are assigned a pre-exhumation maximum temperature of ~242 °C. Lower points in the present topography of the central massif are inferred to have undergone higher temperatures and deeper burial, roughly equivalent to their vertical distance below the highest summits. To translate from temperature to depth, we use our estimate of the initial temperature profile: $T(z) = T_s + g_o z$, where $T_s \approx 8$ °C and $g_o \approx 19.4$ °C/km. Thus, we infer that the rocks that make up the present topography of the central massif originated at depths of about 12.1 to 14.5 km and temperatures of about 242 to 289 °C ("S" and "V" symbols on the initial temperature profile in Fig. 12A).

The intermediate part of the time-depth path is constrained by fission-track closure depths for α-damaged zircon and fluorapatite in the central massif. Note that the onset of exhumation caused the partial annealing zones and the closure depths for both fission-track systems to move upward in the crust because of the increased upward advection of heat caused by exhumation. This effect was countered, but only partially, by an increase in T_c caused by faster cooling. Our analysis of T_c is outlined in the Appendix and accounts for both of these phenomena. Note that published thermal models of the Cascadia margin (e.g., Hyndman and Kang, 1993) are not relevant because they ignore accretion and exhumation.

The method in the Appendix indicates that fission-track ages for α-damaged zircons and fluorapatites of the central massif closed at depths of ~10.0 km and ~4.4 km, respectively. The difference in the closure depths indicates an average exhumation rate of ~0.82 km/m.y. for 14 to 7 Ma (ZA in Fig. 12B). From closure of fluorapatite at ca. 7 Ma to exposure at the Earth's surface at 0 Ma, the average exhumation rate was ~0.66 km/m.y. (AS in Fig. 14B). These rates are not significantly different from those determined by the age-elevation method (ZE and AE in Fig. 12B). In fact, the available evidence suggests that exhumation rates have been relatively constant since middle Miocene time.

The start of exhumation in the central massif can be estimated by calculating how long it took for a point currently at local mean elevation to move upward from an initial depth of accretion of 13.3 km to the α-damaged zircon closure depth of 10 km (Fig. 12B). The difference in depth is 3.3 km, which would take 4.4 m.y. to tra-

verse assuming an average exhumation rate of 0.75 km/m.y. The time-depth plot in Figure 12A shows an age of 13.7 Ma at 10 km depth. Addition of 4.4 m.y. gives an estimate of 18.1 Ma for the initiation of exhumation. Our estimate here assumes that the exhumation rate jumped immediately from 0 to 0.75 km/m.y. at 18 Ma, which would have caused an immediate upward migration of the closure isotherm. We are safe in using a steady-state thermal profile, because after 4.4 m.y., the upward velocity of the closure isotherm should have slowed to within 15% of the exhumation rate (Appendix, Fig. A2). An alternative possibility is that the exhumation accelerated to its average rate of 0.75 km/m.y. over a longer period of time, which would imply an older initiation age. But this option seems unlikely, given that depositional age of the Lower unit of the Olympic subduction complex is about 27 to 19 Ma, which does not permit an initiation age much older than our 18 Ma estimate.

It is interesting to note that areas peripheral to the central massif give younger estimates for the start of exhumation. For example, the sub-Montesano unconformity, which is ~60 km to the south, records the onset of exhumation between 17 and 12 Ma. The fossil partial-annealing zone in the Coast Range terrane (Fig. 10), located ~50 km to the northwest, records the start of exhumation at ca. 12 Ma. These younger ages suggest that the initiation of exhumation was diachronous, starting first in the central massif, then migrating outward with time.

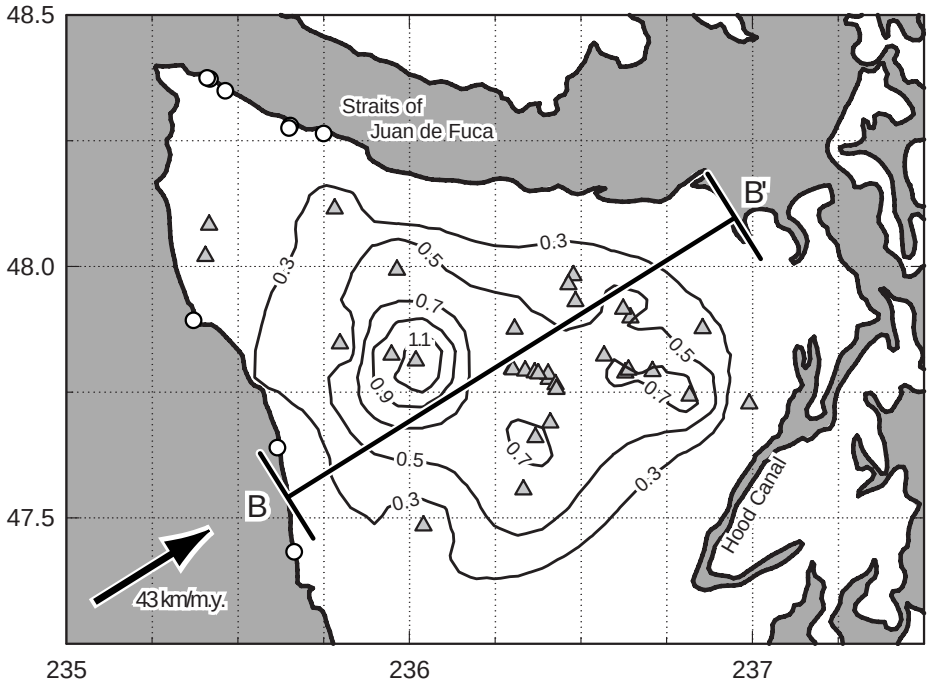

Figure 13. Contour map showing long-term exhumation rates in the Olympic Peninsula area. This map was constructed by determining the depth of closure for each apatite fission-track minimum age using the method outlined in the Appendix, and then dividing the depth by the age to give the local long-term exhumation rate. Apatite localities are shown with circles and triangles, indicating unreset and reset ages, respectively. The 0.3 km/m.y. contour roughly coincides with the base of the fluorapatite partial-annealing zone that existed before the start of exhumation. Rocks outside of this contour are interpreted to have never been buried deeper than ~4.7 km.

Contour Map of Long-Term Exhumation Rates

The method in the Appendix can be used to convert a reset fluorapatite age into an estimate of the local exhumation rate. We focus here on the most recent phase of exhumation, bracketed by closure of fluorapatite fission-track ages and exposure at the Earth's surface. The calculated exhumation rates are reported in the form of a contour map (Fig. 13). Unreset and reset minimum ages are indicated by circles and triangles, respectively. The lowest contour shown in the map is 0.3 km/m.y, which roughly coincides with the base of the fluorapatite partial-annealing zone prior to the start of exhumation. This particular contour was selected because average exhumation rates <0.3 km/m.y. would not be sufficient to expose the base of the fluorapatite partial-annealing zone (~4.7 km depth) over the time interval from middle Miocene time to the present.

The exhumation rate for the central massif area is ~0.7 km/m.y., consistent with the estimate in Figure 12B (AS = 0.66 km/m.y.). However, the highest exhumation rates in the Olympic Mountains, ~1.2 km/m.y., are located west of the central massif. These high rates are indicated by two very young minimum ages (2.3 and 3.9 Ma for Ar^{39} and Ar^{40}, respectively). At present, there are no zircon fission-track ages from this area, so we have no way of knowing how long these high rates have been operating. If rapid exhumation is a relatively recent development (younger than 4 Ma), the total amount of exhumation would be relatively small (~3 to 4 km). Alternatively, if these high rates have been operating since middle Miocene time, we would expect ~20 km of exhumation. There is nothing about the metamorphic grade and deformation fabric of these rocks that would indicate that they have been exhumed from such great depths. Thus, we prefer the interpretation that the high exhumation rates west of the central massif started late in the development of the Olympic Mountains uplift.

DISCUSSION

Tectonic versus Erosional Exhumation

The fission-track data reported here and in Brandon and Vance (1992) have demonstrated that the Olympic Mountains are a site of active uplift and exhumation within the Cascadia forearc high. An important objective of our study has been to document the cause of exhumation in this area. A popular interpretation is that accretionary wedges are most commonly exhumed by extensional deformation operating within the upper levels of the wedge (e.g., Platt, 1986, 1987, 1993; Jayko et al., 1987; Cashman and Kelsey, 1990; Harms et al., 1992; Wallis et al., 1993). An alternative is that exhumation is due to erosion of an emergent forearc high. One of the main observations used to support the tectonic-exhumation model is the recognition that high-pressure metamorphic rocks in accretionary-wedge settings are in some cases overlain by fault zones that have thinned the original metamorphic section. Advocates of the tectonic-exhumation model have argued that "thinning" was produced by extensional faulting. However, it has been noted that contractional thrust faults can attenuate a metamorphic section if the section is tilted rearward before the faults cut through the section (Ring and Brandon, 1994; Wheeler and Butler, 1994). As an example, Ring and Brandon (1994) showed, using kinematic data, that the attenuated metamorphic section on the east side of the

Franciscan Complex could be explained by top-to-the-west thrust faults cutting through an east-dipping metamorphic section.

The tectonic-exhumation model is commonly supported by two other arguments: (1) naturally occurring erosion rates are not fast enough to exhume high-pressure metamorphic rocks within the life span of a typical subduction complex; and (2) it is commonly difficult to account for the volume of sediment produced by erosion. Neither of these arguments is very compelling. Modern erosion rates are usually determined using sediment-yield data for major river basins. These estimates represent an average for an entire drainage, and thus provide only a lower limit for the erosion rates operating in the upland part of the drainage. Nonetheless, a global compilation of sediment-yield data by Milliman and Syvitski (1992) indicates that modern erosion rates can range up to 13 km/m.y. for mountainous areas with small drainages.

As for the second argument, it assumes that the eroded sediment will remain proximal to the uplift, which is typically not the case for both convergent margins and collisional orogens. For example, England (1981) showed that ~55% of the sediment eroded from the European Alps over the past 30 to 40 m.y. was deposited in areas well removed from the orogen, such as deep-sea submarine fans in the Mediterranean. Sediments eroded from the actively deforming New Zealand Alps and Himalaya are mainly transported into deep marine basins (Adams, 1980; Burbank et al., 1993; Curray, 1994). Likewise, much of the sediment eroded from an emergent forearc high is probably transported seaward into slope basins, the trench, or the abyssal plain. Some of this sediment might be trapped in the forearc basin (e.g., Puget Sound) but there would have to be sufficient accommodation space to trap and preserve that sediment. What does get trapped may also be highly diluted by more voluminous sediment coming from the arc and backarc.

We now consider these arguments in the context of the Olympic Mountains. To start, there is no evidence of extensional faulting in the Olympic Mountains. A likely candidate is the Hurricane Ridge fault (Figs. 2 and 4), but it is difficult to envision this structure as a young normal fault given that in most areas the fault is steep to overturned (Fig. 4B). Kinematic indicators have not been found, but the structural style of the fault zone, marked by imbrication and repetition of section, is consistent with the fault having originated as a contractional fault (Fig. 14A). If the Olympic subduction complex was exhumed by normal slip on the Hurricane Ridge fault, then the deepest exposures should currently be directly west of the fault (Fig. 14C). However, the fission-track data show that the area of deepest exhumation is more than 25 km west of the Hurricane Ridge fault (Fig. 4A). Furthermore, the pattern of exhumation is roughly symmetric with the modern topography of the Olympic Mountains, as might be expected if erosional exhumation was the dominant process (Fig. 14B).

Deformation within the Olympic subduction complex is also consistent with a prolonged history of contractional deformation. A prominent pressure-solution cleavage is present in the central and eastern parts of the Olympic subduction complex (Tabor and Cady, 1978b; B. Kang and M. Brandon, unpublished work). Cleavage generally strikes to the northwest at attitudes that fan from moderately east-dipping on the west side of the central massif to moderately west dipping on the east side (Tabor and Cady, 1978b). Where present, the extension direction associated with cleavage is approximately downdip. This pattern of deformation is consistent with horizontal contraction across the Olympic Mountains in a direction parallel to the plate convergence vector, and would have resulted in thickening of the wedge, as indicated by the steeply plunging maximum-extension direction. Our fission-track data indicate that cleavage-related deformation affects rocks as young as early Miocene age and that those rocks remained at temperatures >100 °C until ca. 7 Ma. Thus, we conclude that the deformation associated with cleavage formation was contemporaneous with the uplift and exhumation of the Olympic Mountains. Cleav-

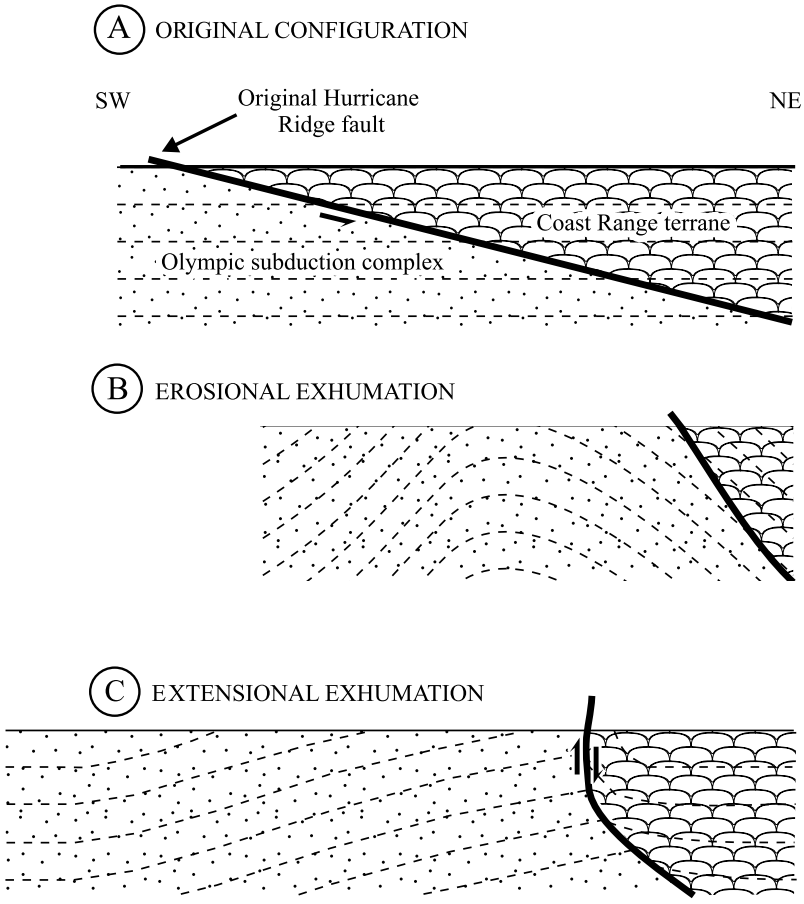

Figure 14. Schematic cross sections illustrating the pattern of exhumation that would result from tectonic and erosional exhumation. (A) The original configuration of the margin was formed by accretion of the Olympic subduction complex beneath the truncated base of the Coast Range terrane. The horizontal dashed lines schematically illustrate depth contours associated with this initial configuration. (B) Erosional exhumation would be distinguished by an exhumation pattern centered over the area of greatest tectonic uplift. In this case, the Hurricane Ridge fault is passively tilted into its present steep orientation. (C) Extensional exhumation caused by normal faulting on the Hurricane Ridge fault would result in an asymmetric pattern with the deepest exposures located directly west of the fault.

age-related deformation probably continues today in the subsurface beneath the forearc high and may be important in controlling uplift of the high (cf. Pavlis and Bruhn, 1983).

Modern Erosion Rates and Sediment Transport Patterns

If the Olympic subduction complex was exhumed mainly by erosion, then we need to consider (1) if modern erosion rates are compatible with our estimates of long-term exhumation rates and (2) if there is a suitable volume of eroded sediment. Table 3 shows a comparison of modern erosion rates with our long-term exhumation rates. We ignore chemical erosion, which is insignificant in this area (average rate is 0.024 km/m.y. for six major basins of the Olympic Mountains; Dethier, 1986). The Elwha and Hoh Rivers drain the northeast and northwest sides of the Olympic Mountains. Sediment yield for the Elwha basin was estimated as part of an environmental impact survey for the removal of a dam at the lower end of the river (B. A. Stoker and D. T. Williams, 1991, written commun.). The area above the dam is entirely in unlogged terrain within Olympic National Park. An inventory of erosion processes indicates an average erosion rate of 0.18 km/m.y. The volume of sediment that has accumulated over the past 61 yr behind the Lake Mills dam indicates an average erosion rate >0.11 km/m.y. Estimates of long-term sediment yield for the Hoh River (Nelson, 1986, p. 18–19) indicate an average erosion rate of 0.32 km/m.y. for its drainage. The lower part of the Hoh River has been logged locally, but the upper part drains natural terrain on the northwest flank of Mount Olympus. Integration of the contour map in Figure 13 indicates that the long-term average erosion rate for the entire Olympic Peninsula has been ~0.28 km/m.y. (Table 3). These data do not reveal any obvious discrepancy between modern erosion rates and long-term exhumation rates when these measurements are compared at the same regional scale.

But where does all the eroded sediment go? The Olympic Mountains are mainly drained by rivers that empty on the west and north sides of the peninsula (Fig. 1). The sediment in those rivers is ultimately transported to more western shelf and slope basins or onto the Cascadia abyssal plain west of the subduction zone (cf. Dickinson and Seely, 1979; Underwood et al., 1980). Plate convergence ensures that the sediments deposited on the abyssal plain will ultimately be carried back into the Cascadia accretionary wedge. Thus, we consider the accretionary wedge itself to be the main repository of sediment eroded from the forearc high.

An interesting observation is that since middle Miocene time, very little sediment has accumulated in the forearc depression east of the Olympic Mountains (Puget Lowland). For example, the Seattle basin (Fig. 2) contains no sediments of middle Miocene through Pliocene age (Fig. 3). About 0.6 km of Pleistocene sediments are present (Johnson et al., 1994), but they are mainly the result of continental glaciation (Booth, 1994). The accommodation space for the Pleistocene sediments is largely accounted for by the postglacial sea-level high. Thus, we concluded that there has been no net tectonic subsidence of the Puget Lowland since early Miocene time. If sediments eroded from the Olympic Mountains were currently being shed eastward into the Puget Lowland, there would be no long-term accommodation space to hold them. Their ultimate fate would be transport through the Straits of Juan de Fuca and into the deep ocean.

Accretion, Deformation, and Erosion Across the Olympic Forearc High

The schematic cross section in Figure 15 shows our concept of how erosion and uplift in the Olympic Mountains are related to deformation within the Cascadia accretionary wedge. The wedge has grown by accretion of sediments from the Cascadia basin that have been driven into the wedge by northeast subduction of the Juan de Fuca plate. Flow lines beneath the continental shelf are shown as parallel and horizontal to account for the fact that the modern shelf basins, such as the Olympic and Willapa–Grays Harbor basins (Fig. 2), have remained close to sea level since late Miocene time and record only minor internal deformation, a point first made by Adams (1984). McNeill et al. (1997) reported an interesting discovery of late Miocene and younger listric normal faults beneath the shelf in an area southwest of the Olympic Peninsula. The cause of the faulting, whether due to deep-seated tectonic processes or to near-surface mass failure, remains unresolved. In either case, the deformation is fairly minor, consisting of ~5 km of horizontal extension over the 50 km width of the shelf since ~15 Ma.

We infer that the shelf basins are moving slowly to the northeast relative to the North American plate due to horizontal shortening within the Olympic Mountains uplift. At the surface, horizontal shortening appears to be mainly localized in the vicinity of the Olympic Mountains uplift. The flow is shown as diverging slightly beneath the Olympic Mountains to account for the fanning of cleavage across the uplift and the presence of east-vergent deformation on the east side of the uplift, as recorded by eastward overturning of the Hurricane Ridge fault and the superjacent Coast Range terrane (Fig. 4B). The continued movement of material into the Olympic Mountains uplift ensures that the mountainous topography and rapid erosion are sustained.

Fission-track data from the central massif indicate a steady rate of exhumation since ca. 14 Ma, which we take as evidence that the topography of the Olympic Mountains forearc has been close to steady-state since that time. To test this conclusion, we examined the section along B–B′ in Figure 13 to see if the accretionary flux at the front of the Cascadia wedge is in balance with the erosional flux from the Olympic Mountains forearc high. An erosional

TABLE 3. AVERAGE MODERN AND LONG-TERM EROSION RATES FOR THE ENTIRE OLYMPIC PENINSULA AREA

Location [references†]	Volume flux* (km^3/m.y.)	Area (km^2)	Erosion rate (km/m.y.)
Modern erosion rates indicated by sediment yield from some Olympic rivers			
Elwha River [1]	114	635	0.18
Hoh River [2]	211	655	0.32
Long-term erosion rates for the entire Olympic Peninsula§ based on apatite fission-track ages			
Outside lowest contour [3]	~650	6504	~0.1
Inside lowest contour [4]	2589	5772	0.45
Total for Peninsula [3,4]	3239	12276	0.26

*Flux is in units of solid rock volume; density is assumed to be 2700 kg/m^3.

§Area of the peninsula is delimited by Hood Canal to the east and the 47°15′ N parallel to the south.

†References: [1] Unpublished environmental impact statement by B. A. Stoker and D. T. Williams (1991) Ebasco Environmental, Washington State; [2] Nelson (1986, p. 18–19), sediment yield increased by 10 percent to account for bed load transport; [3] Average exhumation rate of 0.1 km/m.y. is assumed for area outside of the 0.3 km/m.y. contour in Figure 13; [4] Average exhumation rate for area inside the 0.3 km/m.y. contour as reported in Figure 13.

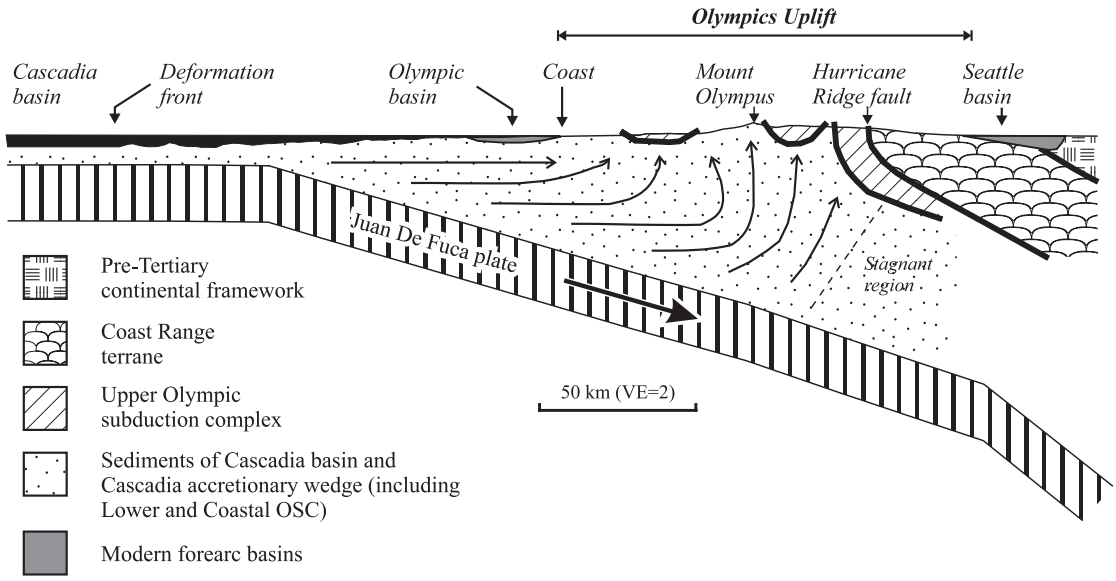

Figure 15. Schematic illustration of flow lines within the Cascadia accretionary wedge. The relationship of adjacent flow lines, whether convergent, parallel, or divergent, indicates the type of strain occurring perpendicular to the flow lines, i.e., contraction, no strain, or extension, respectively. Deformation is considered to be approximately continuous at the scale of the figure, but may involve discontinuous faulting at the local scale. See text for further discussion. OSC—Olympic subduction complex.

flux of 54 km^2/m.y. was determined by integrating the long-term erosion rates determined by fluorapatite fission-track ages along B–B′. Before integration, erosion rates were smoothed and averaged using a moving window that was 30 km wide across the profile and 10 km along the profile. The modern accretionary flux is about 63 km^2/m.y., based on a 2-km-thick incoming sedimentary section (Kulm et al., 1984), an average porosity of 27% (Yuan et al., 1994), and a convergence velocity of 43 km/m.y. (Nishimura et al., 1984). These fluxes are fairly similar and support the idea that the Olympic Mountains segment of the Cascadia margin is currently close to a topographic steady state.

The Olympic Mountains clearly mark an area of anomalous deformation and uplift relative to the rest of the Cascadia convergent margin. A perennial issue is that Olympic Mountains are somehow unusual, and therefore may be unrepresentative of how a "normal" convergent margin would evolve or how the rest of the Cascadia margin is evolving. The more specific question is: Why do uplift and deep exhumation appear to be so strongly concentrated in this segment of the forearc high? Our view is that the Cascadia forearc high is being uplifted and exhumed in a diachronous fashion. There are two factors controlling this process. The first is the flux of accreted sediments into the wedge. The second is slab depth, which controls the amount of material that can be accreted before the forearc becomes emergent, in much the same way that accommodation space controls the thickness of sediment that can accumulate before a sedimentary basin is filled. The accretionary flux along the Cascadia margin increases to the north because of progressive increases in the convergence rate and the thickness of the sediments in the trench. To illustrate, compare the subduction zone west of southern Oregon (43°N), where the normal component of the convergence velocity is 30 km/m.y. and the sedimentary section is 1.25 km thick, with the subduction zone west side of Vancouver Island (49°N), where these values are 43 km/m.y. and 3 km (Kulm et al., 1984; Nishimura et al., 1984; Yuan et al., 1994). This represents about a three-fold increase in the accretionary flux along the length of the margin. The Juan de Fuca slab is anomalously shallow beneath the Olympic Mountains, ~10 km relative to along-strike areas to the north and south (Brandon and Calderwood, 1990). This means less accommodation space for the growing accretionary wedge.

We contend that a high accretionary flux combined with a relatively shallow slab caused the Olympic segment to be the first part of the Cascadia forearc high to emerge above sea level. Early emergence has allowed this part of the forearc high to become more deeply eroded. In adjacent areas, the forearc high has only recently become emergent, but we anticipate that those areas will evolve like the Olympic Mountains, assuming, of course, that there is no change in the rates of convergence and accretion. The diachroneity in the evolution of uplift and exhumation along the length of the forearc high is ~10 to 15 m.y. Diachroneity is a common feature at plate boundaries, but this scale of diachroneity would probably be difficult to recognize at ancient convergent margins. The arguments here support our contention that the Olympic Mountains represent a generalized example of how uplift and erosion can lead to deep exhumation of an emergent forearc high. In this context, it is useful to note that within ~10 to 15 m.y., the Olympic Mountains will be exhumed to a depth equivalent to the deepest part of the Franciscan subduction complex of California, assuming that uplift and erosion continue at their same pace.

CONCLUSIONS

Fission-track dating of detrital apatites from sandstones in subduction complexes can provide useful information about exhumational processes. This kind of work is challenged by the fact that detrital apatites typically produce discordant fission-track results regardless of the degree of thermal resetting. We show that this problem can be overcome by using peak-fitting methods to calculate a minimum age and by having some independent information about depositional age in order to test if the minimum age is reset. The consistency of our results demonstrates the success of this approach.

Apatite fission-track minimum ages reveal a

concentric pattern; the youngest reset ages are clustered around the high topography of the Olympic Mountains, progressively older reset ages are in the foothills of the mountains, and unreset ages are near the Olympic coast. Almost all reset ages are middle Miocene and younger. There are no obvious breaks, as might be expected if exhumation was due to extensional faulting. The pattern indicates systematic variations in erosion rates across the Olympic Mountains, with the fastest rates coinciding with the highest topography.

A stratigraphically coordinated suite of apatite fission-track ages from the Coast Range terrane indicates that prior to the start of exhumation, the base of the fluorapatite partial-annealing zone was located at ~4.7 km depth. The initial thermal gradient was ~19 °C/km, similar to the modern thermal gradient along strike elsewhere in the Cascadia forearc high. Exhumation of the Coast Range terrane in the northwest corner of the peninsula probably started at ca. 12 Ma.

Zircon and apatite fission-track data indicate that exhumation of the central massif of the Olympic Mountains started at ca. 18 Ma and has proceeded at a fairly constant rate of ~0.75 km/m.y. since at least 14 Ma. The total amount of exhumation is judged to be ~12.1 km for the summit regions and ~14.5 km for the deepest valleys of the central massif.

A contour map of exhumation rates, as determined from reset fluorapatite fission-track ages, indicates that the long-term average exhumation rate for the entire Olympic Peninsula area is ~0.26 km/m.y., which is comparable with modern drainage-scale erosion rates of 0.18 to 0.32 km/m.y. estimated from sediment-yield data. The Olympic uplift is mainly drained by west- and northwest-flowing rivers, which ensure that most of the sediment eroded from the uplift is carried into the Pacific Ocean, where it is deposited in slope basins or on the Cascadia abyssal plain seaward of the subduction zone. In the latter case, plate convergence will carry the sediments back into the accretionary wedge. Thus, the accretionary wedge is probably the main repository for sediments eroded from the Olympic uplift. Currently there is a close balance between the influx of accreted sediments and the outflux associated with erosion of the forearc high, which suggests that the topography of the Olympic Mountains segment of the Cascadia margin is close to steady state. Fission-track evidence indicates steady exhumation rates since at least 14 Ma, which suggest that the Olympic Mountains achieved their steady state form shortly after initial emergence above sea level.

ACKNOWLEDGMENTS

Funded by National Science Foundation grants EAR-8707442 and EAR-9005777 (to Brandon); EAR-9117941 (to Roden-Tice and Garver), the Washington State Division of Geology and Earth Resources, Arco, and Yale University. We thank the following individuals for assistance in the field, especially for their help carrying heavy loads in and out of the back country: David Applegate, Arthur Calderwood, Dan Coffey, Jon Einarsen, Jeff Feehan, Martha Goldstyne, Miriam Schoenbaum, Harold Tobin, and packers Kit Neeman and David Johnson. John Aho and Richard Hanson of the Olympic National Park helped with back country logistics. David Applegate, Arthur Calderwood, Linda Neshyba, and Miriam Schoenbaum assisted with mineral separations. Don Miller did some of the fission-track dating during early stages of this project. David Coyle helped with calculation of closure temperatures for fluorapatite using the track-length annealing model. Bruce Stoker of Ebasco Environmental kindly provided information about the modern sediment yield for the Elwha River. Uwe Ring provided comments on an early version of the manuscript. Reviews by Trevor Dumitru, Sarah Roeske, and Jeffrey Unruh helped sharpen the presentation and focus of the paper.

APPENDIX: LONG-TERM EXHUMATION RATES FROM FISSION-TRACK AGES

To estimate long-term exhumation rates from fission-track ages, we need information about the temperature profile and rate of cooling at the time of closure. For the Olympic Mountains, the temperature profile prior to the onset of exhumation is represented by a linear gradient,

$$T(z') = T_s + g_o z'. \quad \text{(A1)}$$

Values for the parameters in equation A1 are estimated above as $T_s \approx 8$ °C and $g_o 1 \approx 19.4$ °C/km. The parameter z' is the effective depth, which is measured relative to the local mean elevation h' of the landscape (Fig. A1). The use of effective depth accounts for the fact that surface topography is generally rougher than the underlying isothermal surfaces (Brown, 1991). Stüwe et al. (1994) showed that as local relief, exhumation rate, and/or thermal gradient increase, the imprint of topography on shallow isotherms becomes more pronounced. In the Olympic Mountains, the local relief, exhumation rate, and thermal gradient are all too small to produce significant short-wavelength distortions in the isothermal surfaces associated with fission-track closure for α-damaged zircon and fluorapatite. In this case, the shallow isotherms will tend to follow the longest wavelengths in the topography. For our case, a practical method for estimating h' is to filter the elevation data so that only the longest wavelengths of the topography remain. For our analysis here, h' was estimated from digital topography that had been low-passed filtered to remove wavelengths less than ~45 km. In the central massif area of the Olympic Mountains, the difference between the original and filtered elevations, $\Delta = h - h' = z - z'$, ranges from –805 m to +1312 m. This approach allows us to address the fact that after a rock passes through the closure isotherm at T_c, the total amount of section that must be eroded to expose the rock at the surface is $z'(T_c) + \Delta$, where $z'(T_c)$ is the depth of the closure isotherm (cf. Brown, 1991)

Exhumation will perturb the initial thermal profile. To model this effect in the Olympic Mountains, we assume that heat flow through the rear part of the wedge can be approximated using a steady-state solution for a one-dimensional layer of thickness L. The upper and lower boundaries of the layer are held at T_s and $T_s + g_o L$, respectively, as indicated by the initial temperature profile. The accretion rate at the base of the layer is equal to the exhumation rate $\dot{\varepsilon}$ at the top of the layer, resulting in a constant advection velocity within the layer. The steady-state temperature profile is given by (equation 8 in Stüwe et al., 1994)

$$T(z, \dot{\varepsilon}) = T_s + g_o L \frac{1 - e^{-\dot{\varepsilon} z'/\kappa}}{1 - e^{-\dot{\varepsilon} L/\kappa}}, \quad \text{(A2)}$$

where κ is the thermal diffusivity. For the sediment-rich

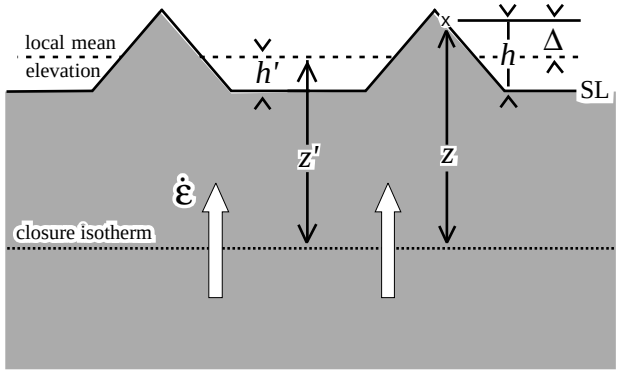

Figure A1. Schematic cross section showing the relationship between surface topography and the depth to the closure isotherm. The exhumation rate $\dot{\varepsilon}$ and topography are assumed to have remained approximately constant with time (i.e., steady-state condition). The closure isotherm, located at a depth z' below the local mean elevation h' of the topography, is assumed to have been relatively flat and stationary when the present land surface passed through the closure isotherm. The total exhumation for a sample collected at an elevation h relative to sea level (SL) is $z = z' + h - h' = z' + \Delta$.

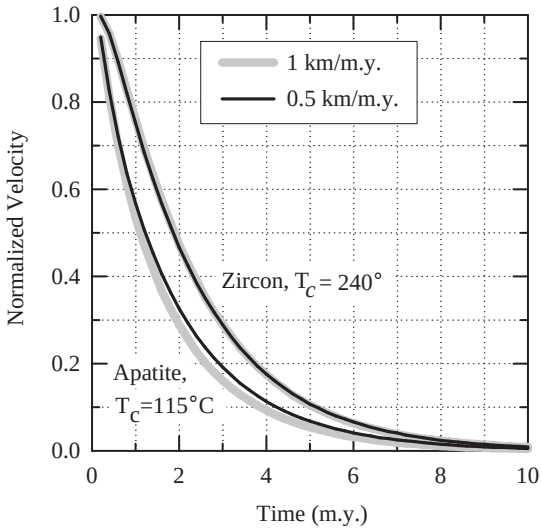

Figure A2. Vertical velocity of the apatite and zircon fission-track (FT) closure isotherms as a function of time since the onset of a steady exhumation rate. Isotherm velocities are normalized to their associated exhumation rate. The examples shown here are for exhumation rates of 0.5 and 1.0 km/m.y. and were calculated using a finite-difference model for a one-dimensional, 20-km-thick layer where the exhumation rate at the top of the layer is equal to the accretion rate at its base. We used the initial temperature profile given by equation A1, a thermal diffusivity of 20 km^2/m.y., and FT closure temperatures (T_c shown in graph) typical for the cooling rate of the Olympic subduction complex (~15 °C/m.y.). These experiments indicate that within 3 to 4 m.y. after exhumation starts, the upward displacement of the closure isotherms slows to velocities <20% of the exhumation rate.

Cascadia accretionary wedge, $\kappa \approx 20$ km^2/m.y. (Brandon and Vance, 1992). Examples below indicate that equation A2 is not particularly sensitive to L as long as it is >~20 km. For our problem here, L is set at 20 km, which approximates the average thickness of the rear part of the accretionary wedge since middle Miocene time.

To use equation A2, we assume that heat flow in the rear part of the wedge has been close to steady state. This implies that the transition to steady state occurred fairly rapidly. This assumption was checked using the Crank-Nicholson finite-difference method (Gerald and Wheatley, 1985, p. 483) to determine the pre-steady-state evolution of the thermal profile. Figure A2 shows the calculated vertical velocity of closure isotherms for α-damaged zircon (~240 °C) and fluorapatite (~115 °C) normalized to the exhumation rate. Note that within 3 to 4 m.y. after the start of exhumation, the vertical velocities of the closure isotherms are <20% of the exhumation rate. The actual normalized velocities of the closure isotherms will be less than estimated here because the calculation used for Figure A2 did not account for the increase in closure temperature that accompanies an increase in the rate of cooling. This effect imparts a small apparent downward velocity to the closure isotherm.

T_c is a function of the rate of cooling $\dot{T} = dT/dt$. An approximate relationship for this effect is given by equation 11 in Dodson (1979):

$$\dot{T} = \frac{-RT_c^2}{E_{50\%} B e^{E_{50\%}/RT_c}}, \quad \text{(A3)}$$

where R is the gas constant, $E_{50\%}$ is the activation energy for 50% annealing, and B is a proportionality constant. Note that the solution of T_c as a function of $\dot{T}$ must be done numerically. The constants in equation A3 can be estimated using annealing data for Durango fluorapatite from Laslett et al. (1987) and for natural α-damaged zircon from Zaun and Wagner (1985) and Tagami et al. (1990). Laslett et al. (1987) reported their annealing data in the form of normalized track lengths, which we converted into normalized track densities using an empirical relation by Green (1988). For Durango fluorapatite: $E_{50\%}$ = 44.65 kcal/mol, and B = 3.223×10^{-26} m.y.; for α-damaged zircon: $E_{50\%}$ = 49.77 kcal/mole, and $B = 3.160 \times 10^{-22}$ m.y. Note that the fluorapatite annealing experiments of Naeser and Faul (1969) give nearly identical predictions for T_c.

The actual cooling rate at closure is a function of the exhumation rate and the vertical gradient in the temperature profile at T_c:

$$\dot{T}(T_c) = \frac{dT}{dz'}\frac{dz'}{dt} = \frac{\dot{\varepsilon}^2}{\kappa}\left(\frac{g_o L}{1 - e^{-\dot{\varepsilon}L/\kappa}} - T_c + T_s\right). \quad \text{(A4)}$$

Equation A2 is inverted to define z_c, the closure depth relative to the true elevation,

$$z_c = \Delta + z_c' = \Delta - \frac{\kappa}{\dot{\varepsilon}} \ln\left(1 - \frac{T_c - T_s}{g_o L}\left(1 - e^{-\dot{\varepsilon}L/\kappa}\right)\right). \quad \text{(A5)}$$

A final equation relates z_c to the fission-track age τ

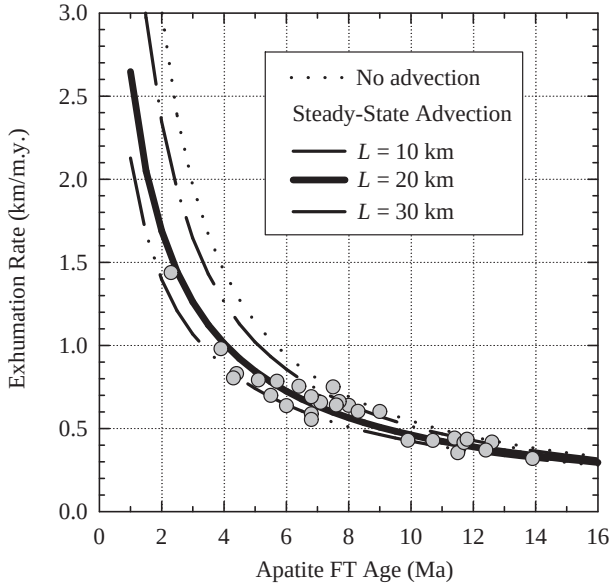

Figure A3. Relationship of fluorapatite fission-track (FT) ages and to the average exhumation rate for the time between closure and exposure at the surface. The exhumation rate is determined by dividing the closure depth by the FT age. To estimate closure depth, we need to account for the initial thermal profile, the perturbation of the initial profile by exhumation, and T_c as a function of cooling rate. The initial temperature profile is given by equation A1 and the thermal diffusivity is set at 20 km^2/m.y. Equation A3 was used to calculate T_c to account for its dependence on cooling rate. The "no advection" example illustrates what would happen if the initial temperature profile remains unchanged during exhumation. The "steady-state advection" examples account for the advection of heat by exhumation. The perturbed temperature profile was approximated using a steady-state solution for a constant exhumation rate (see equation A2). The three steady-state examples illustrate the effect of varying thickness, L, = 10, 20, and 30 km. The data points correspond to the reset minimum ages for Olympic subduction complex apatite samples (Table 2). The variation of the points around the thick solid line (L = 20 km) reflects the fact that in calculating each exhumation rate, there is a difference between the sample's elevation and the local mean elevation (see Fig. A1).

and the constant exhumation rate $\dot{\varepsilon}$,

$$z_c = \dot{\varepsilon}\tau. \quad \text{(A6)}$$

Combining equations A3 with A4 and A5 with [A6] gives two equations that can be solved for the two unknowns, $\dot{\varepsilon}$ and T_c. We used the downhill-simplex method (Press et al., 1992, p. 402) to find a numerical solution.

Figure A3 shows some results of this calculation. The "no advection" case uses the initial temperature profile to calculate a relationship between age and estimated exhumation rate. This example shows the error that occurs by ignoring the advection of heat by exhumation. The concave-upward shape of the curve results from the fact that an increase in the exhumation rate causes an increase in closure temperature and thus an increase in closure depth. The exhumation rates estimated for "steady-state advection" examples are smaller relative to those calculated for the "no advection" case because now we have accounted for the upward displacement of the closure isotherm caused by exhumation. The steady-state profile varies with changing L but not to any significant degree when $L \geq 20$ km. We have chosen to set $L = 20$ km (thick line in Fig. A3) to correspond in an approximate way with the thickness of the wedge over the time interval when exhumation and fission-track closure were occurring. The data points show the actual exhumation rates estimated for the reset minimum ages in Table 2. All points would plot on the thick line ($L = 20$ km) if Δ was everywhere zero.

REFERENCES CITED

Adams, J., 1980, Contemporaneous uplift and erosion of the Southern Alps, New Zealand: Geological Society of America Bulletin, v. 91, Part 2, p. 1–114.

Adams, J., 1984, Active deformation of the Pacific Northwest continental margin: Tectonics, v. 3, p. 449–472.

Armentrout, J. M., 1987, Cenozoic stratigraphy, unconformity-bounded sequences, and tectonic history of southwestern Washington: Washington Division of Geology and Earth Resources Bulletin 77, p. 291–320.

Armentrout, J. M., Hull, D. A., Beaulieu, J. D., and Rau, W. W., 1983, Correlation of Cenozoic stratigraphic units of western Oregon and Washington: Oregon Department of Geology and Mineral Industries, Oil and Gas Investigations 7, 90 p., 1 chart.

Armentrout, J. M., Hintze, L. F., Hull, D. A., Beaulieu, J. D., and Rau, W. W., 1988, Correlation of stratigraphic units of North America–northwest region correlation chart: American Association of Petroleum Geologists, Correlation Chart Series.

Armstrong, R. L., and Ward, P., 1991, Evolving geographic patterns of Cenozoic magmatism in the North American Cordillera: The temporal and spatial association of magmatism and metamorphic core complexes: Journal of Geophysical Research, v. 96, p. 13210–13224.

Babcock, R., Burmester, R., Engebretson, D., Warnock, A., and Clark, K., 1992, A rifted margin origin for the Crescent basalts and related rocks in the northern Coast Range volcanic province, Washington and British Columbia: Journal of Geophysical Research, v. 97, p. 6799–6821.

Bardsley, W. E., 1983, Confidence limits for fission-track dating: Mathematical Geology, v. 15, p. 649–658.

Bence, B. E., and Albee, A. L., 1968, Empirical correction factors for electron microanalyses of silicates and oxides: Journal of Geology, v. 76, p. 382–403.

Bigelow, P. K., 1987, The petrology, stratigraphy, and basin history of the Montesano Formation, southwestern Washington and southern Olympic Peninsula [Masters thesis]: Bellingham, Western Washington University, 263 p.

Booth, D., 1994, Glaciofluvial infilling and scour of the Puget Lowland, Washington, during ice-sheet glaciation: Geology, v. 22, p. 695–698.

Brandon, M. T., 1992, Decomposition of fission-track grain-age distributions: American Journal of Science, v. 292, p. 535–564.

Brandon, M. T., 1996, Probability density plot for fission-track grain-age samples: Radiation Measurements, v. 26, p. 663–676.

Brandon, M. T., and Calderwood, A. R., 1990, High-pressure metamorphism and uplift of the Olympic subduction complex: Geology, v. 18, p. 1252–1255.

Brandon, M. T., and Vance, J. A., 1992, New statistical methods for analysis of fission-track grain-age distributions with applications to detrital zircon ages from the Olympic subduction complex, Western Washington State: American Journal of Science, v. 292, p. 565–636.

Brown, R. W., 1991, Backstacking apatite fission-track stratigraphy: A method for resolving the erosional and isostatic rebound components of tectonic uplift histories: Geology, v. 19, p. 74–77.

Burbank, D. W., Derry, L. A., and France-Lanord, C., 1993, Reduced Himalayan sediment production 8 Myr ago despite an intensified monsoon: Nature, v. 364, p. 48–50.

Carlson, W. D., 1990, Mechanisms and kinetics of apatite fission-track annealing: American Mineralogist, v. 75, p. 1120–1139.

Cashman, S., and Kelsey, H., 1990, Forearc uplift and extension, southern Hawke's Bay, New Zealand; mid-Pleistocene to present: Tectonics, v. 9, p. 23–44.

Clowes, R. M., Brandon, M. T., Green, A. G., Yorath, C. J., Sutherland Brown, A., Kanasewich, E. R., and Spencer, C., 1987, LITHOPROBE–southern Vancouver Island: Cenozoic subduction complex imaged by deep seismic reflections: Canadian Journal of Earth Sciences, v. 24, p. 31–51.

Crowley, K. D., Cameron, M., and McPherson, B. J., 1990, Annealing of etchable fission-track damage in F-, OH-, Cl-, and Sr-apatite 1. Systematics and preliminary interpretation: Nuclear Tracks and Radiation Measurements, v. 17, p. 409.

Crowley, K. D., Cameron, M., and Schaefer, R. L., 1991, Experimental studies of annealing of etched fission tracks in fluorapatite: Geochimica et Cosmochimica Acta, v. 55, p. 1449–1465.

Curray, J. R., 1994, Sediment volume and mass beneath the Bay of Bengal: Earth and Planetary Science Letters, v. 125, p. 371–383.

Dethier, D. P., 1986, Weathering rates and the chemical flux from catchments in the Pacific Northwest, USA, *in* Colman, S. M., and Dethier, D. P., eds., Rates of chemical weathering of rocks and minerals: Orlando, Florida, Academic Press, p. 503–530.

Dickinson, W. R., and Seely, D. R., 1979, Structure and stratigraphy of forearc regions: American Association of Petroleum Geologists Bulletin, v. 63, p. 2–31.

Dodson, M. E., 1976, Closure temperature in cooling geochronological and petrological systems: Contributions to Mineralogy and Petrology, v. 40, p. 259–274.

Dodson, M. E., 1979, Theory of cooling ages, *in* Jaeger, E., and Hunziker, J. C., eds., Lectures in isotope geology: Berlin, Springer-Verlag, p. 194–202.

Donelick, R., Ketcham, R., and Carlson, W., 1998, Calibration of fission track annealing in apatite, *in* Naeser, C., Dokka, R., and Naeser, N., eds., Fission-track thermochronology: Geological applications: Berlin, Springer Verlag (in press).

Duddy, I. R., Green, P. F., and Laslett, G. M., 1988, Thermal annealing of fission tracks in apatite, 3. Variable temperature behavior: Chemical Geology (Isotope Geoscience Section) v. 73, p. 25–38.

Duncan, R. A., 1982, A captured island chain in the Coast Range of Oregon and Washington: Journal of Geophysical Research, v. 87, p. 10827–10837.

Engebretson, D. C., Gordon, R. G., and Cox, A., 1985, Relative motions between oceanic and continental plates in the Pacific basin: Geological Society of America Special Paper 206, 59 p.

England, P., 1981, Metamorphic pressure estimates and sediment volumes for the Alpine orogeny: An independent control on geobarometers?: Earth and Planetary Science Letters, v. 56, p. 387–397.

Foster, D., Kohn, B., and Gleadow, A., 1996, Sphene and zircon fission track closure temperatures revisited; empirical calibrations from $^{40}Ar/^{39}Ar$ diffusion studies of K-feldspar and biotite, *in* International Workshop on Fission Track Dating: Gent, University of Gent, 26–30/8, p. 37.

Galbraith, R. F., 1981, On statistical models for fission-track counts: Journal of Mathematical Geology, v. 13, p. 471–478.

Galbraith, R. F., 1988, Graphical display of estimates having differing standard errors: Technometrics, v. 30, p. 271–281.

Galbraith, R. F., 1990, The radial plot: Graphical assessment of spread in ages: Nuclear Tracks and Radiation Measurements, v. 17, p. 207–214.

Galbraith, R. F., and Green, P. F., 1990, Estimating the component ages in a finite mixture: Nuclear Tracks and Radiation Measurements, v. 17, p. 197–206.

Galbraith, R. F., and Laslett, G., 1993, Statistical models for mixed fission track ages: Nuclear Tracks and Radiation Measurements, v. 21, p. 459–470.

Garver, J. I., and Brandon, M. T., 1994, Erosional denudation of the British Columbia Coast Ranges as determined from fission-track ages of detrital zircon from the Tofino basin, Olympic Peninsula, Washington: Geological Society of America Bulletin, v. 106, p. 1398–1412.

Gerald, C. F., and Wheatley, P. O., 1985, Applied Numerical Analysis (third edition): Reading, Massachusetts, Addison-Wesley, 579 p.

Green, P. F., 1981, A new look at statistics in fission-track dating: Nuclear Tracks and Radiation Measurements, v. 5, p. 77–86.

Green, P. F., 1988, The relationship between track shortening and fission-track age reduction in apatite: Combined influences of inherent instability, annealing anisotropy, and length bias and system calibration: Earth and Planetary Science Letters, v. 89, p. 335–352.

Green, P. F., Duddy, I. R., Gleadow, A. J. W., and Tingate, P. R., 1985, Fission track annealing in apatite: Track length measurements and the form of the Arrhenius plot: Nuclear Tracks and Radiation Measurements, v. 10, p. 323–328.

Green, P. F., Duddy, I. R., Gleadow, A. J. W., and Lovering, J. F., 1989, Apatite fission-track analysis as a paleotemperature indicator for hydrocarbon exploration, *in* Naeser, N. D., and McCulloh, T. H., eds., Thermal history of sedimentary basins: New York, Springer-Verlag, p. 181–195.

Harms, T., Jayko, A. S., and Blake, M. C., 1992, Kinematic evidence for extensional unroofing of the Franciscan Complex along the Coast Range fault zone, northern Diablo Range, California: Tectonics, v. 12, p. 228–241.

Harrison, T. M., Armstrong, R. L., Naeser, C. W., and Harakal, J. E., 1979, Geochronology and thermal history of the Coast plutonic complex, near Prince Rupert, British Columbia: Canadian Journal of Earth Sciences, v. 16, p. 400–410.

Heller, P. L., Tabor, R. W., and Suczek, C. A., 1987, Paleogeographic evolution of the United States Pacific Northwest during Paleogene time: Canadian Journal of Earth Sciences, v. 24, p. 1652–1667.

Hurford, A. J., 1986, Cooling and uplift patterns in the Lepontine Alps, south central Switzerland, and an age of vertical movement on the Insubric fault line: Contributions to Mineralogy and Petrology, v. 92, p. 413–427.

Hurford, A. J., and Green, P. F., 1983, The zeta age calibration of fission-track dating: Chemical Geology (Isotope Geoscience Section), v. 1, p. 285–317.

Hyndman, R. D., and Wang, K., 1993, Thermal constraints on the zone of major thrust earthquake failure: The Cascadia subduction zone: Journal of Geophysical Research, v. 98, p. 2039–2060.

Jayko, A. S., Blake, M. C., and Harms, T., 1987, Attenuation of the Coast Range ophiolite by extensional faulting, and nature of the Coast Range "thrust," California: Tectonics, v. 6, p. 475–488.

Johnson, S. Y., Potter, C. J., and Armentrout, J. M., 1994, Origin and evolution of the Seattle fault and Seattle basin, Washington: Geology, v. 22, p. 71–74.

Kasuya, M., and Naeser, C. W., 1988, The effect of α-damage on fission-track annealing in zircon: Nuclear Tracks and Radiation Measurements, v. 14, p. 477–480.

Ketcham, R., Donelick, R., and Carlson, W., 1998, Numerical modeling of fission track annealing in apatite, *in* Naeser, C., Dokka, R., and Naeser, N., eds., Fission-track thermochronology: Geological applications: Berlin, Springer Verlag (in press).

Kulm, L. D., et al., eds., 1984, Western North American continental margin and adjacent ocean floor off Oregon and Washington, Ocean Margin Drilling Program, Regional Atlas Series, Volume 1: Woods Hole, Massachusetts, Marine Science International, 32 p.

Laslett, G. M., Green, P. F., Duddy, I. R., and Gleadow, A. J. W., 1987, Thermal annealing of fission tracks in apatite 2. A quantitative analysis: Chemical Geology (Isotope

Geoscience Section) v. 65, p. 1–13.
Lonsdale, P., 1988, Paleogene history of the Kula plate: Offshore evidence and onshore implications: Geological Society of America Bulletin, v. 100, p. 733–754.
McNeill, L., Piper, K., Goldfinger, C., Kulm, L., and Yeats, R., 1997, Listric normal faulting on the Cascadia continental margin: Journal of Geophysical Research, v. 102, p. 12123–12138.
Miller, D. S., Duddy, I. R., Green, P. F., Hurford, A. J., and Naeser, C. W., 1985, Results of interlaboratory comparison of fission-track age standards: Nuclear Tracks and Radiation Measurements, v. 10, p. 381–391.
Milliman, J. D., and Syvitski, J. P. M., 1992, Geomorphic/tectonic control of sediment discharge to the ocean: The importance of small mountainous rivers: Journal of Geology, v. 100, p. 525–544.
Muller, J. E., 1977, Geology of Vancouver Island: Geological Survey of Canada Open File Map 463, scale 1:250 000.
Naeser, C., and Faul, H., 1969, Fission-track annealing in apatite and sphene: Journal of Geophysical Research, v. 74, p. 705–710.
National Geophysics Data Center, 1989, Geophysics of North America: Release 1.1: Boulder, Colorado, National Oceanic and Atmospheric Administration, CD-ROM data files.
Nelson, L. M., 1986, Fluvial sediment in the Hoh River, *in* Lum, W. E., II, Reconnaissance of the water resources of the Hoh Indian Reservation and the Hoh River basin, Washington, U.S. Geological Survey Water Resources Investigations Report 85–4018, p. 18–19.
Nishimura, C., Wilson, D. S., and Hey, R. N., 1984, Pole of rotation analysis of present-day Juan de Fuca plate motion: Journal of Geophysical Research, v. 89, p. 10283–10290.
Orange, D. L., 1990, Criteria helpful in recognizing shear-zone and diapiric mélanges: Examples from the Hoh accretionary complex, Olympic Peninsula, Washington: Geological Society of America Bulletin, v. 102, p. 935–951.
Orange, D. L., and Underwood, M., 1995, Patterns of thermal maturity as diagnostic criteria for interpretation of mélanges: Geology, v. 23, p. 1144–1148.
Orange, D. L., Geddes, D., and Moore, J., 1993, Structural and fluid evolution of a young accretionary complex: The Hoh rock assemblage of the western Olympic Peninsula, Washington: Geologic Society of America Bulletin, v. 105, p. 1053–1075.
O'Sullivan, P., and Parrish, R., 1995, The importance of apatite composition and single-grain ages when interpreting fission track data from plutonic rocks: A case study from the Coast Ranges, British Columbia: Earth and Planetary Science Letters, v. 132, p. 213–224.
Palmer, S. P., and Lingley, W. S., Jr., 1989, An assessment of the oil and gas potential of the Washington outer continental shelf: University of Washington, Washington Sea Grant Program, 83 p.
Pavlis, T. L., and Bruhn, R. L., 1983, Deep-seated flow as a mechanism for the uplift of broad forearc ridges and its role in the exposure of high P/T metamorphic terranes: Tectonics, v. 2, p. 473–497.
Platt, J. P., 1986, Dynamics of orogenic wedges and the uplift of high-pressure metamorphic rocks: Geological Society of America Bulletin, v. 97, p. 1037–1053.
Platt, J. P., 1987, The uplift of high-pressure-low temperature metamorphic rocks: Royal Society of London Philosophical Transactions, ser. A, v. 321, p. 87–103.
Platt, J. P., 1993, Exhumation of high pressure metamorphic rocks: A review of concepts and processes: Terra Nova, v. 5, p. 119–133.
Press, W. H., Teukolsky, S. A., Vetterling, W. T., and Flannery, B. P., 1992, Numerical recipes in Fortran: The art of scientific computing: Cambridge, Cambridge University Press, 963 p.
Rau, W. W., 1973, Geology of the Washington coast between Point Grenville and the Hoh River: Washington Department of Natural Resources, Geology and Earth Resources Division Bulletin no. 66, 58 p.
Rau, W. W., 1975, Geologic map of the Destruction Island and Taholah quadrangles, Washington: Washington Department of Natural Resources, Geology and Earth Resources Division, Geologic Map GM-13, scale 1:62 500.
Rau, W. W., 1979, Geologic map in the vicinity of the Lower Bogachiel and Hoh River Valleys, and the Washington Coast: Washington Department of Natural Resources, Geology and Earth Resources Division, Geologic Map GM-24, scale 1:62 500.
Ring, U., and Brandon, M. T., 1994, Kinematic data for the Coast Range fault and implications for exhumation of the Franciscan subduction complex: Geology, v. 22, p. 735–738.
Sherrod, D. R., and Smith, J. G., 1989, Preliminary map of upper Eocene to Holocene volcanic and related rocks of the Cascade Range, Oregon: U.S. Geological Survey Open-File Report 89-14, scale 1:500 000 , 20 p.
Shouldice, D. H., 1971, Geology of the Western Canadian continental shelf: Canadian Petroleum Geology Bulletin, v. 19, p. 405–436.
Smith, J. G., 1989, Geologic map of upper Eocene to Holocene volcanic and related rocks in the Cascade Range, Washington: U.S. Geological Survey Open-File Report 89-311, scale 1:500 000, 61 p.
Snavely, P. D., Jr., 1987, Tertiary geologic framework, neotectonics, and petroleum potential of the Oregon-Washington continental margin, *in* Scholl, D. W., Grantz, A., and Vedder, J. G., eds., Geology and resource potential of the continental margin of western North America and adjacent ocean basins—Beaufort Sea to Baja California: Houston, Texas, Circum-Pacific Council for Energy and Mineral Resources, Earth Science Series, v. 6, p. 305–335.
Snavely, P. D., Jr., and Kvenvolden, K., 1989, Geology and hydrocarbon potential, *in* Preliminary evaluation of the petroleum potential of the Tertiary accretionary terrane, west side of the Olympic Peninsula, Washington: U.S. Geological Survey Bulletin 1892, p. 1–17.
Snavely, P. D., Jr., Neim, A. R., MacLeod, N. S., Pearl, J. E., and Rau, W. W., 1980, Makah Formation—A deep marginal basin sequence of late Eocene and Oligocene age in the northwestern Olympic Peninsula, Washington: U.S. Geological Survey Professional Paper 1162, 38 p.
Snavely, P. D., Jr., Rau, W. W., and Hafley, D. J., 1986, Tertiary Foraminiferal localities in the Cape Flattery area, northwestern Olympic Peninsula, Washington: U.S. Geological Survey Open-File Report 86-344A, 18 p.
Snavely, P. D., Jr., MacLeod, N. S., and Niem, A. R., 1993, Geologic map of Cape Flattery, Clallam Bay, Ozette Lake, and Lake Pleasant quadrangles, northwestern Olympic Peninsula, Washington: U.S. Geologic Survey Miscellaneous Investigations Series I-1946, scale 1:48 000.
Sneyd, A. D., 1984, A computer program for calculating exact confidence intervals for ages in fission-track dating: Computers and Geoscience, v. 10, p. 339–345.
Squires, R. L., Goedert, J. L., and Kaler, K. L., 1992, Paleontology and stratigraphy of Eocene rocks at Pulali Point, Jefferson County, Eastern Olympic Peninsula, Washington: Washington Division of Geology and Earth Resources Report of Investigations 31, 27 p.
Stewart, R. J., 1970, Petrology, metamorphism, and structural relations of graywackes in the Western Olympic Peninsula, Washington [Ph.D. dissert.]: Stanford, California, Stanford University, 129 p.
Stüwe, K., White, L., and Brown, R., 1994, The influence of eroding topography on steady-state isotherms. Applications to fission track analysis: Earth and Planetary Science Letters, v. 124, p. 63–74.
Suczek, C., Babcock, R., and Engebretson, D. C., 1994, Tectonostratigraphy of the Crescent terrane and related rocks, Olympic Peninsula, Washington, *in* Swanson, D., and Haugerud, R., eds., Geologic field trips in the Pacific Northwest: 1994 Geological Society of America Annual Meeting, p. 1H1–1H11.
Tabor, R. W., and Cady, W. H., 1978a, Geologic map of the Olympic Peninsula: U.S. Geological Survey Map I-994, scale 1:125 000.
Tabor, R. W., and Cady, W. H., 1978b, The structure of the Olympic Mountains, Washington—Analysis of a subduction zone: U.S. Geological Survey Professional Paper 1033, 38 p.
Tagami, T., and Dumitru, T., 1996, Provenance and thermal history of the Franciscan accretionary complex: Constraints from zircon fission track thermochronology: Journal of Geophysical Research, v. 101, no. B5, p. 11353–11364.
Tagami, T., and Shimada, C., 1996, Natural long-term annealing of the zircon fission track system around a granitic pluton: Journal of Geophysical Research, v. 101, no. B4, p. 8245–8255.
Tagami, T., Ito, H., and Nishimura, S., 1990, Thermal annealing characteristics of spontaneous fission tracks in zircon: Chemical Geology (Isotope Geoscience Section), v. 80, p. 159–169.
Tagami, T., Carter, A., and Hurford, A., 1996, Natural long-term annealing of the zircon fission-track system in Vienna Basin deep borehole samples; constraints upon the partial annealing zone and closure temperature: Chemical Geology, v. 130, no. 1–2, p. 147–157.
Underwood, M. B., Bachman, S. B., and Schweller, W. J., 1980, Sedimentary processes and facies associations within trench and trench-slope settings, *in* Field, M. E., Bouma, A. H., and Colburn, I., eds., Quaternary depositional environments on the Pacific continental margin: Pacific Section, Society of Economic Paleontologists and Mineralogists, p. 211–229.
Wagner, G. A., and Van Den Haute, P., 1992, Fission-track dating: Dordrecht, Netherlands, Kluwer Academic Publishers, 285 p.
Wagner, G. A., Reimer, G. M., and Jäger, E., 1977, Cooling ages derived by apatite fission-track, mica Rb-Sr and K-Ar dating: The uplift and cooling history of the Central Alps: University of Padova, Institute of Geology and Mineralogy Memoir, v. 30, 27 p.
Wallis, S., Platt, J., and Knott, S., 1993, Recognition of synconvergence extension in accretionary wedges with examples from the Calabrian Arc and the Eastern Alps: American Journal of Science, v. 293, p. 463–494.
Walsh, T. J., Korosec, M. A., Phillips, W. M., Logan, R. L., and Schasse, H. W., 1987, Geologic map of Washington—Southwest quadrant: Washington Division of Geology and Earth Resources Geologic Map GM-34, scale 1:250 000 and 28 p.
Wells, R. E., Engebretson, D. C., Snavely, P. D., Jr., and Coe, R. S., 1984, Cenozoic plate motions and the volcanotectonic evolution of western Oregon and Washington: Tectonics, v. 3, p. 275–294.
Wessel, P., and Smith, W. H. F., 1991, Free software helps map and display data: Eos (Transactions, American Geophysical Union), v. 72, p. 441, p. 445–446.
Wheeler, J., and Butler, R. W. H., 1994, Criteria for identifying structures related to true crustal extension in orogens: Journal of Structural Geology, v. 16, p. 1023–1027.
Wilson, D. S., 1988, Tectonic history of the Juan de Fuca Ridge over the last 40 million years: Journal of Geophysical Research, v. 93, p. 11863–11876.
Yamada, R., Tagami, T., Nishimura, S., and Ito, H., 1995, Annealing kinetics of fission tracks in zircon: An experimental study: Chemical Geology (Isotope Geoscience Section), v. 122, p. 249–58.
Yuan, T., Spence, G., and Hyndman, R., 1994, Seismic velocities and inferred porosities in the accretionary wedge sediments at the Cascadia margin.: Journal of Geophysical Research, B, Solid Earth and Planets, v. 99, p. 4413–4427.
Zaun, P. E., and Wagner, G. A., 1985, Fission-track stability in zircons under geological conditions: Nuclear Tracks and Radiation Measurements, v. 10, p. 303–307.

MANUSCRIPT RECEIVED BY THE SOCIETY JANUARY 20, 1995
REVISED MANUSCRIPT RECEIVED APRIL 30, 1997
MANUSCRIPT ACCEPTED SEPTEMBER 29, 1997

Printed in U.S.A.